



**HAL**  
open science

## **Bioinspired co-polyesters of hydroxy-fatty acids extracted from tomato peel agro-wastes and glycerol with tunable mechanical, thermal and barrier properties**

Mathilde Marc, Regis Risani, Eric Desnoes, Xavier Falourd, Bruno Pontoire,  
Rúben Rodrigues, Rita Escórcio, Ana Paula Batista, Romain Valentin,  
Nathalie Gontard, et al.

### ► **To cite this version:**

Mathilde Marc, Regis Risani, Eric Desnoes, Xavier Falourd, Bruno Pontoire, et al.. Bioinspired co-polyesters of hydroxy-fatty acids extracted from tomato peel agro-wastes and glycerol with tunable mechanical, thermal and barrier properties. *Industrial Crops and Products*, 2021, 170, pp.113718. 10.1016/j.indcrop.2021.113718 . hal-03318668

**HAL Id: hal-03318668**

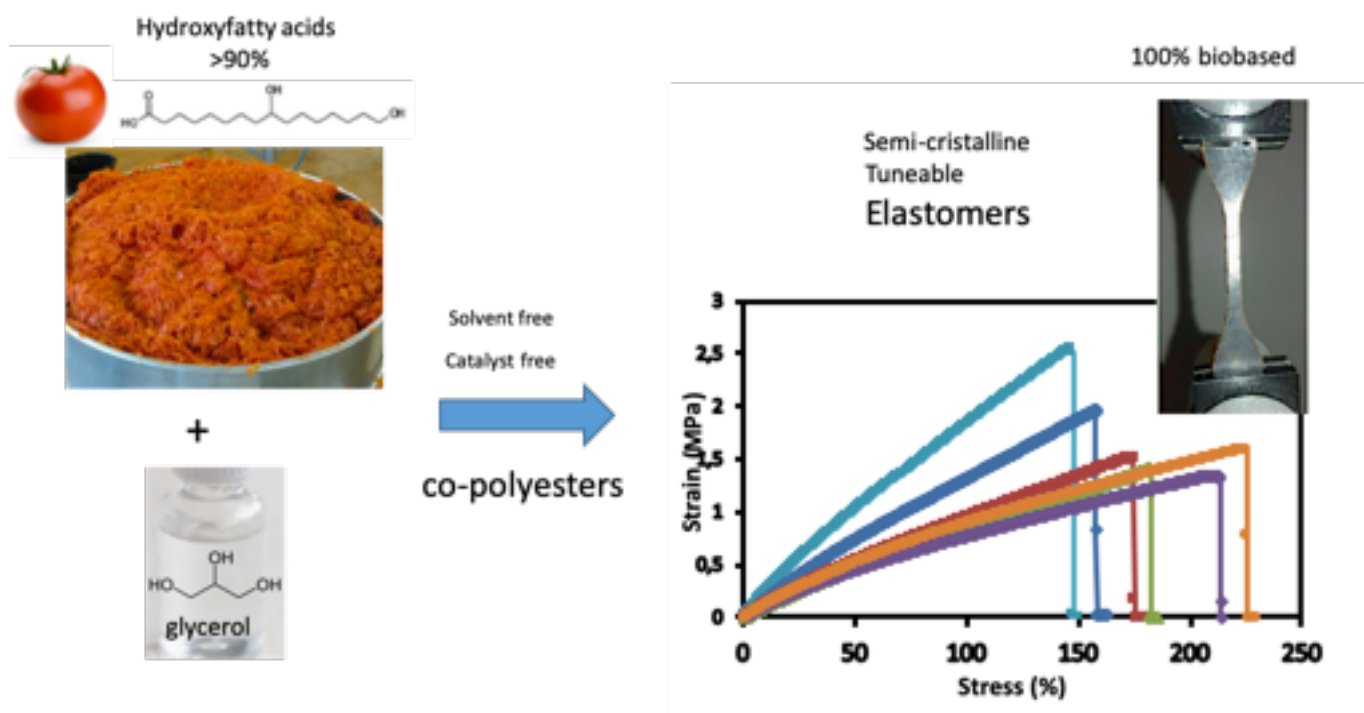
**<https://hal.inrae.fr/hal-03318668v1>**

Submitted on 7 Oct 2022

**HAL** is a multi-disciplinary open access archive for the deposit and dissemination of scientific research documents, whether they are published or not. The documents may come from teaching and research institutions in France or abroad, or from public or private research centers.

L'archive ouverte pluridisciplinaire **HAL**, est destinée au dépôt et à la diffusion de documents scientifiques de niveau recherche, publiés ou non, émanant des établissements d'enseignement et de recherche français ou étrangers, des laboratoires publics ou privés.

# Graphical abstract



1

2

3 **Bioinspired co-polyesters of hydroxy-fatty acids extracted from tomato peel agro-wastes and glycerol**  
4 **with tunable mechanical, thermal and barrier properties**

5

6

7 Mathilde Marc<sup>†</sup>, Regis Risani<sup>†</sup>, Eric Desnoes<sup>†</sup>, Xavier Falourd<sup>†,¶</sup>, Bruno Pontoire<sup>†</sup>, Rúben Rodrigues<sup>&</sup>, Rita  
8 Escórcio<sup>&</sup>, Ana Paula Batista<sup>‡</sup>, Romain Valentin<sup>§</sup>, Nathalie Gontard<sup>‡</sup>, Cristina Silva Pereira<sup>&</sup>, Christelle  
9 Lopez<sup>†</sup>, Eric Leroy<sup>!</sup>, Denis Lourdin<sup>†</sup>, Didier Marion<sup>†</sup>, Bénédicte Bakan<sup>†\*</sup>.

10

11

12 <sup>†</sup> Biopolymers Interactions Assemblies Research Unit 1268 (BIA), INRAE, Rue de la Géraudière, 44316,  
13 Nantes, France

14 <sup>‡</sup> Agropolymers Engineering and Emerging Technologies Joint Research Unit 1208 (IATE), INRAE-CIRAD-  
15 SupAgro-University of Montpellier, 2 place Viala, Montpellier, 34000, France

16 <sup>§</sup> Agro-Industrial Chemistry Joint Research Unit 1010 (LCA), INRAE-INP-ENSIACET, 4 Allée Emile Monso,  
17 Toulouse, 31000, France

18 <sup>¶</sup> Biopolymers and Structural Biology platform (BIBS), BIA research unit, INRAE, rue de la Géraudière,  
19 Nantes, 44300, France

20 <sup>!</sup> Université de Nantes. Oniris. CNRS. GEPEA. UMR 6144, 44600 Saint Nazaire, France.

21 <sup>&</sup> Instituto de Tecnologia Química e Biológica António Xavier, Universidade Nova de Lisboa (ITQB NOVA),  
22 Av. da República, Oeiras, 2780-157, Portugal.

23

24 \*corresponding author: benedicte.bakan@inrae.fr

25

26 **Highlights**

- 27
- High yield extraction process enables recovering unique fatty acids from cutin-rich agro-
- 28 industrial byproducts.
- 29
- Polyesters biobased and bioinspired by native cutin are synthesized by co-polymerization
- 30 of fatty acid extracts and glycerol
- 31
- Tuning the amount of esterified glycerol induced modification in the macromolecular
- 32 structure and crystallinity.
- 33
- Resulting modified properties comprise elastomer like mechanical behavior (with up to
- 34 200% elongation), a decrease in O<sub>2</sub> permeability, and an increase in anti-biofouling
- 35 properties

36

37

38

39 **Abstract**

40 By mimicking the cutin natural polyester networks of plant cuticles, we produced hydrophobic elastomers  
41 by a sustainable process, i.e., using a catalyst- and solvent-free polycondensation of glycerol and hydroxy  
42 fatty acids, two by-products of the agro-food industry. The hydroxy fatty acid fraction was obtained by  
43 ethanolic alkaline hydrolysis of cuticle from industrial tomato. This industrial-like fatty acid fraction  
44 contained more than 90% wt. of 9(10)-16 dihydroxyhexadecanoic acid (diOHC16). The co-polyesters were  
45 designed by increasing the ratio of esterified glycerol/diOHC16 in a range observed in plant cutins (up to  
46 6% wt.). Their structure and functional properties (thermal, mechanical, gas permeability, interaction with  
47 bacterial cells) were characterized. Increasing the glycerol contents induced a significant decrease in the  
48 crosslink density of the polyesters and the formation of crystalline domains with a hexagonal organization.  
49 These structural modifications were related to a marked increase of elastomeric extensibility (up to 217%).  
50 While water vapor permeability was not impacted, the increase of glycerol content induced a significant  
51 decrease in oxygen permeability. None of the polyesters displayed biocide activity, but an increase of  
52 glycerol content significantly reduced the adhesion of bacterial cells, potentially giving rise to antifouling  
53 applications.

54

55 **Keywords**

56 Tomato cuticle, biomimetic, cutin polyester, hydroxy fatty acid, glycerol, semi-crystalline elastomer

57

## 58        **1. Introduction**

59        To face terrestrial life colonization, plants have developed a hydrophobic barrier, the cuticle, that covers  
60        the surface of their aerial organ. This ubiquitous interface between the plant and its environment fulfills  
61        multiple crucial functions such as mechanical supports against wounding and cracks, control of non-  
62        stomatal water loss, and permeation of gases (Fich et al., 2016).

63                The main biopolymer in this complex hydrophobic assembly is the cutin polyester, which is essential  
64        for the functional properties of the plant cuticle (Nawrath, 2006; Yeats and Rose, 2013). Plant cutin is  
65        insoluble due to its polyester network architecture. It can be depolymerized mainly into a variety of long-  
66        chain hydroxy fatty acids building blocks. Each of these carboxylic acid monomers contains 16 and-or 18  
67        carbon atoms and one to three hydroxyl groups. Interestingly, the tomato fruit peels concentrate a high  
68        amount of cutin, whose monomer composition is strikingly homogenous, with about 80% by weight  
69        consisting of 9(10)-16 dihydroxyhexadecanoic acid (diOHC16). The remaining minor cutin components,  
70        especially phenolics, mono- and di-carboxylic acids probably play an important role in the insoluble  
71        polyester crosslinked network. Indeed, pure diOHC16 is an AB<sub>2</sub> type molecule (with A being a carboxylic  
72        acid function and B a hydroxyl group). The polyesterification of such a single monomer would typically lead  
73        to hyperbranched macromolecules that are easily soluble in common organic solvents (Feast and Stainton,  
74        1995; Testud et al., 2017).

75                However, this  $\omega$ -hydroxylated molecule carrying midchain functionalities, presents high interfacial  
76        properties (Fameau et al., 2013) and constitutes a unique opportunity for the development of innovative  
77        biosourced polymer materials from depolymerized tomato cutin feedstock (Heredia-Guerrero et al., 2017).  
78        Reaching this innovation would address the important landmarks set by the United Nations sustainable  
79        development goals because tomato cutin is a readily available residue of the tomato processing industries.

80 Tomato wastes, i.e., pomaces, are mainly composed of peels and seeds. 44 MT of tomato fruit are  
81 processed worldwide, to make derived tomato products (e.g., purees, juice, sauces) generating nearly 1.5  
82 MT of animal feed and production of biogas whereas their transformation for development of new  
83 materials, from bioplastic to high-functional value products remains largely overlooked (Fritsch et al.,  
84 2017). Peels and seeds can be easily separated and dried, directly in the factory, and the hydroxy fatty  
85 acids can be easily extracted from the cutin of tomato peels (Benítez et al., 2018).

86 Furthermore, glycerol, the main by-product of the biodiesel and oil industries (Quispe et al., 2013),  
87 has been identified as a potentially influential minor component in tomato cutin. Esterified glycerol has  
88 been evidenced in the cutin polyester network structure (Graça et al., 2002) and typically represents only  
89 0.6 to 0.7 % wt. of the cutin monomers obtained by depolymerization (Philippe et al., 2016). Besides, we  
90 have recently highlighted that the ratio of glycerol to hydroxy fatty acid can be modulated in tomato fruit.  
91 Indeed, in tomato fruit mutants affected in a cutin synthase (CUS1), an enzyme involved in the cutin  
92 biosynthesis, a 60% reduction in cutin deposition was induced without any significant negative impact  
93 either on the fruit development or the generation of cracks (Girard et al., 2012). Looking at the cutin  
94 polyester structure, we observed a significant increase of the glycerol to hydroxy fatty acid ratio. These  
95 results obtained with the mutants suggested that the inclusion of co-polymerized glycerol in the tomato  
96 cutin network could be involved in the mechanical adaptation of the fruit cuticle, in particular in the  
97 modulation of its extensibility. This is especially essential for resistance to turgor pressure during fruit  
98 growth and environmental constraints to prevent fruit from cracking, a phenomenon responsible for major  
99 crop losses (Barker, 1988). Taking inspiration from nature, our leading hypothesis is that we can produce  
100 tunable bio-based co-polyesters that mimic potential adaptive events of cutin simply by playing on the  
101 glycerol/diOHC16 ratio.

102 Hereinafter, we describe a solvent- and catalyst-free polymerization process to generate co-  
103 polyesters from two diOHC16 and glycerol, two readily available and renewable biological resources.  
104 Tuning of the ratio of esterified glycerol to diOHC16 in a range similar to what it is observed in plant cutin  
105 effectively results in the modulation of the structure (amorphous or semi-crystalline), the properties  
106 (mechanical, thermal, and barrier properties) of the ensuing co-polyesters.

107

## 108 2. Experimental Section

### 109 2.1. Materials

110 Glycerol (99 % purity) and all other chemical ACS reagents were from Sigma-Aldrich (USA). The analytical  
111 grade solvents were obtained from Carlo Erba (Val de Reuil, France). The 16-10(9)-hydroxy-hexadecanoic  
112 acid-enriched fraction (referred to as “diOHC16” in the manuscript) was extracted from industrial tomato  
113 samples provided by the “Conserveries de Bergerac” (UNIPROLEDI, Bergerac, France). The peels and seeds  
114 of the pomaces were separated by decantation in a water tank. The floating peels were recovered, their  
115 water excess was squeezed out and then dried at room temperature. Dried peels (1kg) were grounded and  
116 dewaxed under the reflux of acetone: ethanol 1:1 (v:v) in a Soxhlet extractor and then dried in a fume  
117 hood. Cutin depolymerization was conducted at room temperature in 5% (wt.) KOH in ethanol 95%. After  
118 filtration on a Buchner funnel, about 90% of the filtrate was evaporated under vacuum and replaced by  
119 water. Hydroxy fatty acids were precipitated by adjusting pH at 3.5 with concentrated HCl. The hydroxy  
120 fatty acid precipitate was extensively washed with water, and finally freeze-dried.

121 The purity of the fatty acids was determined after phase partitioning in  $\text{CHCl}_3/\text{CH}_3\text{OH}/\text{H}_2\text{O}$  8:4:3  
122 (v:v). The lower chloroform-rich phase containing only lipophilic compounds, mainly fatty acids and some  
123 pigments, was recovered, evaporated under vacuum, and weighed. The colored cutin monomer batches

124 contain  $98 \pm 0.5\%$  of lipophilic compounds. The fatty acid composition of the lipophilic fraction was  
125 determined by gas chromatography coupled to a mass spectrometer as previously described (Philippe et  
126 al., 2020). A 60% yield of hydroxy fatty acids was obtained and the same batch of 500g of diOHC16 extract  
127 was used in the study. This batch was dark-red colored due to the remaining pigments and highly  
128 concentrated in diOHC16 (90% of the hydroxy fatty acids) (**Supplemental Figure 1**).

129

## 130 **2.2. Preparation of the cutin-like co-polyesters films**

131 Co-polyesters films were produced by a solvent-free and catalyst-free polycondensation. We developed a  
132 polymerization process to minimize the non-esterified glycerol within the copolyester films. Preparation  
133 of different weight ratio of diOHC16/ Glycerol (1.8g diOHC16 for PG0 ; 1.71g diOHC16/90 mg glycerol for  
134 PG2.3; 1.62g diOHC16/180 mg glycerol for PG3.9; 1.53g diOHC16/ 270 mg glycerol for PG4.8 ; 1.44g  
135 diOHC16/ 360 mg glycerol for PG5.2 and 1.35 g of diOHC16/ 450 mg glycerol for PG6.2 respectively) were  
136 put in Teflon molds (5cm x 5cm) with a thickness of about 0.7-1 mm. The nomenclature of the co-polyesters  
137 refers to the glycerol weight ratio comprised within the co-polyester at the end of the process (**Table 1**).

138 Bulk poly-condensation was then conducted for 24h at 150°C in an oven (VaccuTherm, ThermoFisher,  
139 USA). To avoid bubbles and to minimize the presence of residual free glycerol, i.e., non-esterified, in the  
140 final material a 400mbar vacuum was applied during the first 2h of the polycondensation process. After  
141 24h, the polymers were rapidly cooled on ice and stored at room temperature. Samples of the ensuing  
142 films were immersed under agitation in various solvents of diOHC16 and/or of glycerol, i.e., water, ethanol,  
143 and chloroform 16h at room temperature to assess their solubility.

144

## 145 **2.3. Structural characterization of the cutin-like co-polyester films**

146 Attenuated total reflectance Fourier-transform infrared spectroscopy (ATR-FTIR) spectra (200 scans) were  
147 recorded at a resolution of  $2\text{ cm}^{-1}$  on a Nicolet Magna IR 550 spectrometer equipped with a liquid nitrogen-  
148 cooled mercury-cadmium-telluride detector. The instrument was continuously purged with dry air.  
149 Spectra of co-polyester films were obtained by attenuated total reflection (ATR) using a single reflection  
150 accessory fitted with a thermostated diamond crystal with a  $45^\circ$  angle of light incidence. All spectra (3 per  
151 co-polyester) were acquired in the  $4000$  to  $700\text{ cm}^{-1}$  range at  $4\text{ cm}^{-1}$  resolution and accumulating 30 scans.

152  $^{13}\text{C}$  solid-state NMR (CP-MAS NMR) was carried out on a Bruker AvanceIII-400 MHz spectrometer  
153 operating at  $100.61\text{ MHz}$  for  $^{13}\text{C}$ , equipped with a double-resonance H/X CP-MAS 4-mm probe for CP-MAS  
154 (cross-polarization magic-angle-spinning) solid-state experiments. Sixty mg of the co-polyester films were  
155 put packed into 4 mm zirconia rotors. The samples were spun at  $12,000\text{ Hz}$  at room temperature. CP-MAS  
156 spectra were acquired with a contact time of  $1\text{ ms}$ , a recycling delay of  $10\text{ s}$ , and over-accumulation of  
157 2048 scans. The carbonyl carbon was set to  $176.03\text{ ppm}$  through external glycine calibration. NMR spectra  
158 deconvolution was performed using the PeakFit<sup>®</sup> software (Systat Software, Inc., USA).

159 X-Ray Diffraction analysis was performed on a Bruker-AXS D8 Discover diffractometer. The X-ray  
160 beam was produced in a sealed copper tube at  $40\text{ kV}$  and  $40\text{ mA}$ . The  $500\text{-}\mu\text{m}$  beam with a  $\text{CuK}\alpha_1$   
161 wavelength ( $1.5405\text{ \AA}$ ) was collimated and parallelized using two crossed-coupled Göbel mirrors. The X-  
162 ray diffraction data were collected using a Vantec500 two-dimensional detector, previously calibrated with  
163 silver behenate, in the  $2\theta$ -range:  $3\text{-}70^\circ$ . The samples are placed perpendicular to the X-ray beam. Recorded  
164 diffractograms  $I = f(2\theta)$  were normalized to remove the influence of thickness variation among the  
165 samples. Temperature kinetics were performed using Linkam's HFS91 stage. The samples were placed in a  
166 mica window cell. The detector was positioned at a focusing distance of  $8.6\text{ cm}$  from the sample surface.

167 It was in a direct beam position. The heating kinetic applied to the sample was  $3^{\circ}\text{C}\cdot\text{min}^{-1}$  from  $20^{\circ}\text{C}$  to  
168  $100^{\circ}\text{C}$ .

169

#### 170 **2.4. Chemical characterization of the cutin-like co-polyester films**

171 Free glycerol was extracted from polymers (5mg in 1 mL of  $\text{CH}_3\text{OH}$ ), overnight at room temperature.  
172 Esterified glycerol was released from polymers by mild methanolysis using a modified procedure (Graça et  
173 al., 2002). Isolated pieces of the co-polyester films were stirred at room temperature in a mixture of 50mM  
174 sodium methoxide in dry methanol with the internal standard 1,2,3-butanetriol (Shen and Xu, 2013). Free  
175 and esterified glycerol extracts were dried with a nitrogen flow and analyzed by GC-MS and GC FID. For  
176 the quantification of the cutin hydroxy fatty acids, the co-polyesters were depolymerized through  
177 methanolysis during 6h until complete depolymerization. The depolymerized hydroxy fatty acids were  
178 silylated with 1% BSTFA/TMCS and analyzed by GC-MS and GC-FID as previously described (Philippe et al.,  
179 2016).

180 Free OH groups were derivatized by benzyl-etherification resistant to alkaline depolymerization,  
181 according to an established method (Philippe et al., 2016). Briefly, co-polyesters (3mg) were mixed at  $90^{\circ}\text{C}$   
182 in a screw-capped glass tube for 24h with 15mg of 2-benzyloxy-1-methylpyridinium triflate and 1.68 mg of  
183 magnesium oxide in 1mL of trifluorotoluene. The samples were then extensively washed with  $\text{CH}_2\text{Cl}_2$  and  
184 dried before depolymerization and cutin monomer analysis. GC-FID surface response of the  
185 labeled diOHC16 (either in midchain position or in  $\omega$ -position) were compared between the different co-  
186 polyesters and were expressed as equivalent of heptadecanoic acid, as an external standard.

187

#### 188 **2.5. Thermal and mechanical properties of the cutin-like co-polyester films**

189 Differential Scanning Calorimetry (DSC) was performed on a DSC Q100 (TA Instruments, New Castle, DE,  
190 USA). The DSC instrument was calibrated with an indium standard. Analyses were made with 2–5mg of  
191 samples, using hermetically-sealed aluminum pans. An empty pan was used as a reference. Samples were  
192 cooled from 20°C to –50°C and heated at 3°C.min<sup>-1</sup> until 80°C. The Glass transition temperature (T<sub>g</sub>) of the  
193 co-polyesters was defined at the midpoint of heat capacity change on the thermograms recorded on the  
194 first scan. The melting temperature was determined at the maximum of the peak.

195 Dynamic Mechanical Thermal Analysis (DMTA) was performed on a DMTA MKIV (Rheometric  
196 Scientific, US). Rectangular specimens (20 mm × 4 mm) were cut from the films and thickness of about 0.7-  
197 1 mm was precisely measured with a micrometer. The samples were analyzed in the tensile mode at the  
198 frequency of 1 Hz with a strain amplitude of 0.1%. To keep the samples taut a static force superior by 10%  
199 to the dynamic force was applied to the sample. A scanning rate of 3°C min<sup>-1</sup> from -50°C to 80 °C was used.  
200 Each sample was analyzed in duplicate.

201 The tensile test of the films was carried out using MTS Synergie 100 (MTS Systems Corporation,  
202 USA). The film samples were cut into a dog-bone shape. The test was performed using a cross-head speed  
203 of 10 mm/min. The reported results, including Young’s modulus, ultimate strength, and elongation at  
204 break, were the average values of five specimens. The standard deviations are indicated in **Table 1**.

205

## 206 **2.6. Barrier properties of the cutin-like co-polyester films**

207 Water permeances of the co-polyesters were determined at 25°C and under 100% relative humidity  
208 gradient using transpiration chambers as previously described (Philippe et al., 2016; Schreiber L and J,  
209 2009). Typically, co-polyesters (5 replicates) were mounted on the top of the transpiration chamber with  
210 a 0.6 cm diameter hole, subsequently filled with 300 µL of deionized water, inverted, and placed in a

211 desiccator filled with a desiccant. Water transfer across the co-polyesters samples was determined by  
212 gravimetric analysis of the transpiration chamber every 8h during 4 days. Water permeance (P) was  
213 calculated as the ratio  $P=F/A.\Delta c$ , where F (Flow rate of water) is determined as the slope of water transfer  
214 across the samples (in  $\text{g.s}^{-1}$ ), A (in  $\text{m}^2$ ) is the area across which transport has occurred, and  $\Delta c$  (in  $\text{g.m}^{-3}$ ) is  
215 the water gradient driving force.

216 The oxygen permeability of co-polyesters was determined in triplicate at 23°C and 0% relative  
217 humidity through an isostatic and dynamic method using gas-phase chromatography as previously  
218 described (Motedayen et al., 2019). The film samples (4 cm diameter) were placed inside sealed stainless-  
219 steel permeability cells. The lower chamber was continuously spread by a  $5 \text{ mL.min}^{-1}$  flux of permeant gas  
220 ( $\text{O}_2$ ), and the upper chambers by the same flux of vector gas (helium), thus applying a permanent  $\text{O}_2$  partial  
221 pressure difference. The permeability cells were coupled to a gas chromatograph with a thermal  
222 conductivity detector (GC-TCD, Agilent 7890A, USA), equipped with an automatic valve to online analyze  
223 the evolution with time of  $\text{O}_2$  gas concentration in the upper chamber. The GC-TCD was equipped with two  
224 capillary columns - PoraPlot U (25 m  $\times$  0.530 mm id, Agilent) and HP Molesieve (30 m  $\times$  0.535 mm id,  
225 Agilent) – able to separate  $\text{O}_2$ ,  $\text{CO}_2$  and  $\text{N}_2$ . Data were collected and processed using the ChemStation  
226 OpenLab Software (Agilent) and SRA Prochem interface (SRA Instruments). The  $\text{O}_2$  permeability,  $P_{\text{O}_2}$   
227 ( $\text{mol.m}^{-1}.\text{s}^{-1}.\text{Pa}^{-1}$ ), of the film samples was calculated as follows:

228 
$$P_{\text{O}_2} = \frac{J \times e}{A \times \Delta P} \quad (\text{equation1})$$

229 Where:  $J$  ( $\text{mol.s}^{-1}$ ) is the flux of gas that passes through the film,  $e$  is the film thickness (m),  $A$  is the  
230 permeation area ( $\text{m}^2$ ) and  $\Delta P$  is the  $\text{O}_2$  pressure differential between the upper and lower chambers of the  
231 cell (Pa).

232

## 233 **2.7. Microbiological analyses**

234 *S. aureus* NCTC8325 and *E. coli* TOP 10 cells ( $10^5$  cells·mL<sup>-1</sup>) in Mueller-Hinton broth (MHB) medium were  
235 exposed for 24h to 0.5 cm<sup>2</sup> of polyester films (*ca.* 10 to 20 mg·mL<sup>-1</sup>) at 37 °C, under orbital agitation (100  
236 rpm). Upon incubation, the cellular morphology and the viability of the bacterial cells were visualized by  
237 light and fluorescent microscopy, respectively, using a Leica DM6000 B microscope equipped with an iXon  
238 EM+ 885 EMCCD camera (Andor Technology®). The fluorescent dye propidium iodide (PI) was used for  
239 labeling the dead cells (red fluorescence). Negative controls, i.e., bacteria growing in media devoid of cutin-  
240 like co-polyester films, were also carried out. Films from each tested condition were also collected to scan  
241 for the presence of bacterial cells on the film's surface. All assays were done in triplicate. The films were  
242 first washed with phosphate-buffered saline (PBS) to remove non-adherent bacteria, subsequently fixed  
243 with glutaraldehyde 2.5% (v/v) during 10 min. After 10 min, samples were rinsed with distilled water and  
244 dehydrated with aqueous solutions with increasing concentrations of ethanol (ranging from 70 to 100%).  
245 Scanning electron microscopy (SEM) (microscope JEOL JSM-7001F, with an accelerating voltage set to 15  
246 kV) was used to scan the co-polyester film's surfaces. All samples were coated with gold before analysis.

247

## 248 **3. Results and Discussion**

### 249 **3.1. Sustainable production of dark black colored insoluble co-polyesters with different ratio of** 250 **esterified-glycerol**

251 The cutin-like polyesters were manufactured to meet green chemistry and sustainability criteria. Indeed,  
252 they were prepared through a catalyst- and solvent-free process using hydroxy fatty acids and glycerol  
253 from renewable resources, i.e. by-products of the tomato and oilseed processing industries. The  
254 biorefinery process designed for the recovery ion of the hydroxy fatty acids from tomato pomaces leads

255 to higher yield and purity than the existing processes described in the literature (Benítez et al., 2018;  
 256 Cogognigni et al., 2014). First, fractionation of tomato pomaces into seeds and peels was conducted. This  
 257 opens ways for the valorization of both seeds and peels and prevents seed lipids co-extraction. Indeed,  
 258 seeds contain more than 30% oil (Giannelos et al., 2005). In contrast with previous studies starting from raw  
 259 pomaces, the extraction of fatty acids from peels provided a fatty acid fraction with a higher diOHC16  
 260 content (90% instead of 45% (Tedeschi et al., 2018). The hydrolytic process of the tomato cutin polyester  
 261 was conducted at room temperature and used green solvents, i.e., water and ethanol, which can be  
 262 recycled to improve the sustainability of the process. Interestingly, the ethanolic alkaline hydrolysis at  
 263 room temperature gave rise to a high fatty acid yield (around 60% wt. of dry peels), instead of around 15%  
 264 wt. for hot aqueous alkaline hydrolysis (Cogognigni et al., 2014), thereby strengthening the sustainability  
 265 of the process. Considering that tomato cuticle contains about 70% of cutin and 30% of polysaccharides  
 266 (Philippe et al., 2020), this means that our biorefinery process recovered more than 85% of the available  
 267 cutin monomers in the tomato pomaces.

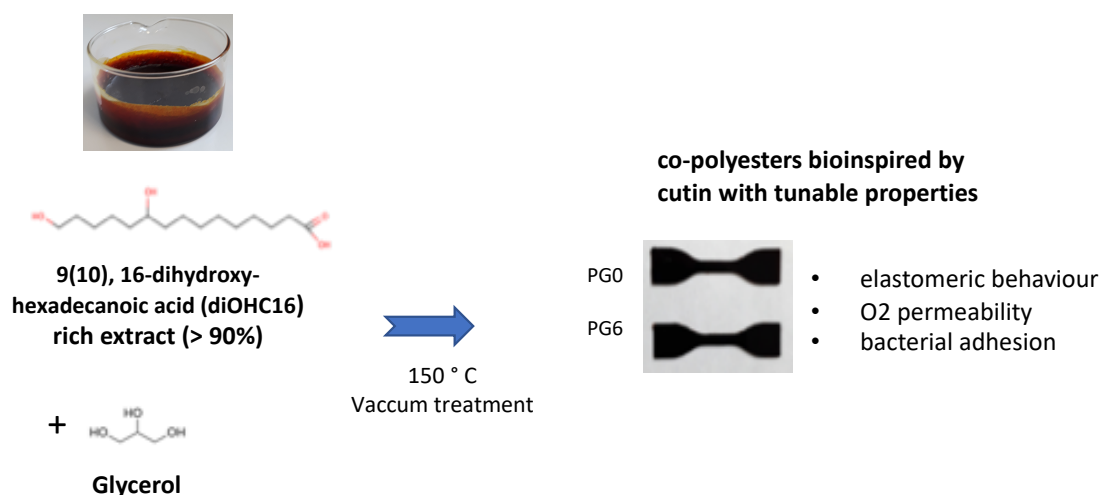


**Figure 1 – Solvent- and catalyze-free polycondensation of tomato cutin extract and glycerol**

268

269 The cutin monomers extract consisted of ~90 % diOHC16 and were dark-red colored as for existing  
270 processes (Benítez et al., 2018) due to the remaining pigments. According to the FTIR and UV spectra, these  
271 pigments contain phenolic compounds(Aleixandre-Tudo and du Toit, 2018; Benítez et al., 2018; Heredia-  
272 Guerrero et al., 2014; Herrera et al., 1998) (supplemental Figure 1). The cutin-like co-polyesters formed by  
273 polycondensation of the diOHC16-rich hydroxy fatty acid extract and glycerol (**Figure 1**) displayed a dark  
274 brown color. They were insoluble in water, ethanol, and chloroform (**Table 1**) as previously reported for  
275 polyesters synthesized from lower purity tomato hydroxy fatty acids extracts (Benítez et al., 2018; Benitez  
276 et al., 2015). The cutin monomers extracts were highly rich in lipophilic compounds (98%). Accordingly,  
277 the insolubility of our films suggests that, as in native plant cutin, the minor lipidic compounds, i.e.,  
278 dicarboxylic fatty acids, and co-extracted phenolic molecules (supplemental Figure 1) could participate in  
279 the polymerization process. The participation of these compounds in the polyester crosslinked network  
280 should compensate for the AB2 structure of the diOHC16 which should normally lead to branched  
281 polymers soluble in organic solvents (Feast and Stainton, 1995; Testud et al., 2017).

282 In previous works on fatty acid extracts containing 9,10,16-trihydroxypalmitic or 9,10-  
283 dihydroxystearic acids (Benitez et al., 2015), the authors pointed out the capacity of such molecules to  
284 form two additional carboxylic acid functions by an oxidative diol cleavage reaction of the 9,10 neighbor  
285 hydroxyl groups. This would increase the acid/hydroxyl ratio and allow the formation of crosslinked  
286 insoluble polyester networks. In our case, despite oxidation reactions evidenced by the darkening that  
287 occurs during the polymerization process (**Figure 1**), no such fatty acids with vicinal hydroxyl groups are  
288 present in the diOHC16-rich extract (**supplemental Figure 1**).

289 Finally, the objective of the present study was to focus on the modulating effect of glycerol on the  
290 properties of the co-polyesters produced from the fatty acid extract from peels provided by tomato

291 pomaces, in line with a vision of sustainable biobased and cutin-inspired chemistry. Therefore, the same  
292 cutin monomer batch was used and materials containing different amounts of esterified glycerol were  
293 produced. After the poly-condensation reaction, the added glycerol can be (i) free, i.e., non-esterified,  
294 acting as an external plasticizer, or (ii) esterified, constituting a polyester monomer. Determination of free  
295 and esterified glycerol contents revealed that more than 95% of the glycerol was esterified (**Table 1**).

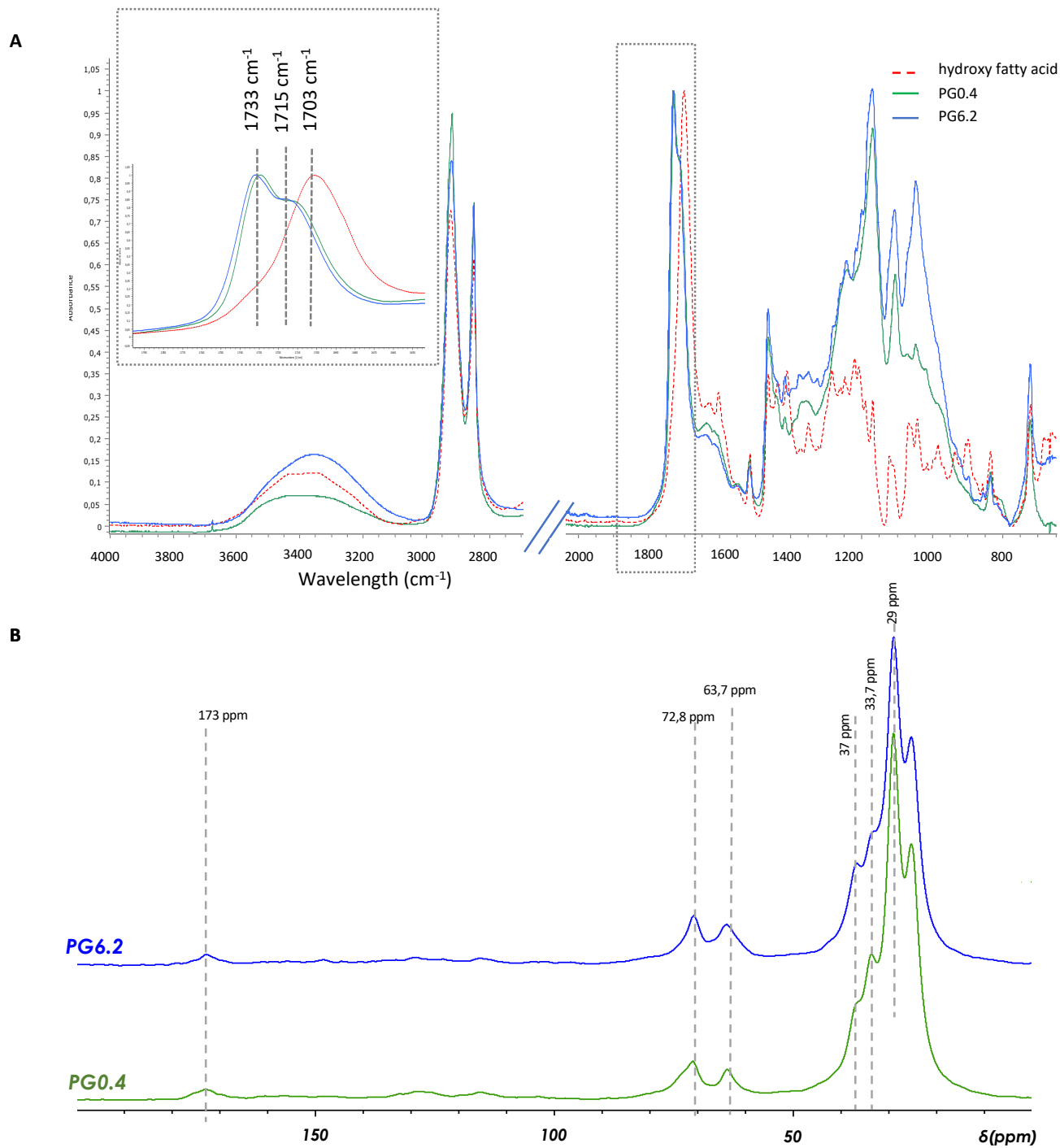
W water, CF chloroform, Et Ethanol

Table 1 Composition, chemical, thermal and mechanical characterization of the cutin-inspired co-polyesters

Sample	Chemical characterisation						DSC					DMTA		Mechanical test		
	glycerol total (%wt)	esterified glycerol (% wt)	free glycerol (% wt)	insoluble fraction (%) W	insoluble fraction (%) CF	insoluble fraction (%) Et	Glass transition temperature (°C)	Melting temperature 1 (°C)	Melting Enthalpy (J/g)	Melting temperature 2 (°C)	Melting Enthalpy (J/g)	Mechanical relaxation temperature (°C)	Storage Modulus at 50°C (MPa)	Breaking stress (MPa)	Strain at break (%)	Young's modulus (Mpa)
<b>PG0.4</b>	0.43 ± 0.24	0.38 ± 0.21	0.05 ± 0.04	100	100	98	-8.7	-	-	-	-	8.6	5.867	2.1 ± 0.5	124.0 ± 24.5	2.29 ± 0.05
<b>PG2.3</b>	2.27 ± 0.31	2.17 ± 0.32	0.10 ± 0.03	99	100	98	-13.1	-	-	-	-	5.4	5.035	2.0 ± 0.2	155 ± 12.7	1.74 ± 0.06
<b>PG3.9</b>	3.93 ± 0.34	3.75 ± 0.31	0.18 ± 0.05	99	99	94	-15.7	-	39.7	0.07	-	3.2	4.058	1.7 ± 0.2	180.7 ± 10.3	1.26 ± 0.2
<b>PG4.8</b>	4.80 ± 0.82	4.57 ± 0.80	0.23 ± 0.15	99	97	95	-17.0	17.9	41.6	0.32	2.60	1.9	1.408	1.4 ± 0.1	178.4 ± 8.6	1.11 ± 0.03
<b>PG5.2</b>	5.20 ± 0.31	4.87 ± 0.5	0.32 ± 0.2	99	94	91	-20.4	16.8	41.2	2.04	7.96	0.9	1.521	1.3 ± 0.1	197.3 ± 21.1	1.10 ± 0.01
<b>PG6.2</b>	6.18 ± 0.39	5.89 ± 0.45	0.29 ± 0.1	100	88	80	-18.5	18.3	41.6	0.59	9.05	0.2	1.589	1.5 ± 0.1	217.6 ± 14.2	1.19 ± 0.08

297       **3.2. A gradual increase of the glycerol content induces a decrease in the branching of the co-**  
298               **polyester films**

299 The co-polyesters containing the lowest (PG0.4) and the highest (PG6.2) levels of esterified glycerol were  
300 characterized by ATR- FTIR and  $^{13}\text{C}$  NMR (**Figure 2**). ATR-FTIR indicated the formation of esters bonds in  
301 these co-polyesters. Indeed, we observed the characteristic shift of the carbonyl band from  $1705\text{ cm}^{-1}$ ,  
302 assigned to the carboxylic acid, to the  $1733\text{ cm}^{-1}$  band assigned to the esterified carbonyl (Heredia-Guerrero  
303 et al., 2014). In addition, the  $1715\text{ cm}^{-1}$  band assigned to the ester bond involved in hydrogen bonding was  
304 also evidenced, as previously observed in tomato cutin (Girard et al., 2012). In our present co-polyesters,  
305 the hydrogen bonds could involve the free hydroxyl groups either from the hydroxy fatty acids and/or from  
306 the esterified glycerol. Besides, the  $1171\text{ cm}^{-1}$  band assigned to the stretching vibration of the C-O-C ester  
307 bond was observed in all co-polyesters. Likewise, the  $^{13}\text{C}$  C-MAS (**Figure 2B**) data confirmed the formation  
308 of esters, evidenced by a single broad peak at 173 ppm and by the peak at 64 ppm, which is assigned to  
309 primary esters (Tedeschi et al., 2018). Furthermore, no significant free fatty acid signals were evidenced at  
310 178 ppm (-COOH) and 35 ppm (-CH<sub>2</sub>-COOH). Finally, the comparison of the surface ratio of the 33.7 ppm  
311 and 37 ppm peaks, assigned to aliphatic carbons (-CH<sub>2</sub>-CHOR-CH<sub>2</sub>-) and (CH<sub>2</sub>-CHOH-CH<sub>2</sub>) respectively  
312 (Benitez et al., 2015), indicated a decrease (40%) in the esterification of the secondary hydroxyls of  
313 diOHC16 associated with the increase in the glycerol content.



**Figure 2- ATR-FTIR and NMR spectra of the cutin-like polyesters films**

**A** . ATR-FTIR spectra of hydroxy-fatty acid (diOHC16) extracted from tomato cutin and the corresponding polymers with high ( PG6.2) or low ( PG0.4) glycerol. In inset, the magnification of the CO stretching bands at 1733  $\text{cm}^{-1}$  and 1715  $\text{cm}^{-1}$  are assigned respectively to ester group, and ester bond interacting by hydrogen bond whereas the band at 1703  $\text{cm}^{-1}$  is assigned to carboxylic group.

**B**. Solid State  $^{13}\text{C}$  CP-MAS NMR spectra of the polymers

315 The reticulation of the co-polyesters was further monitored by the chemical labeling of the free OH  
316 groups by benzyl ether within the diOHC16-derived polyesters (Philippe et al., 2016) (**Figure 3**).

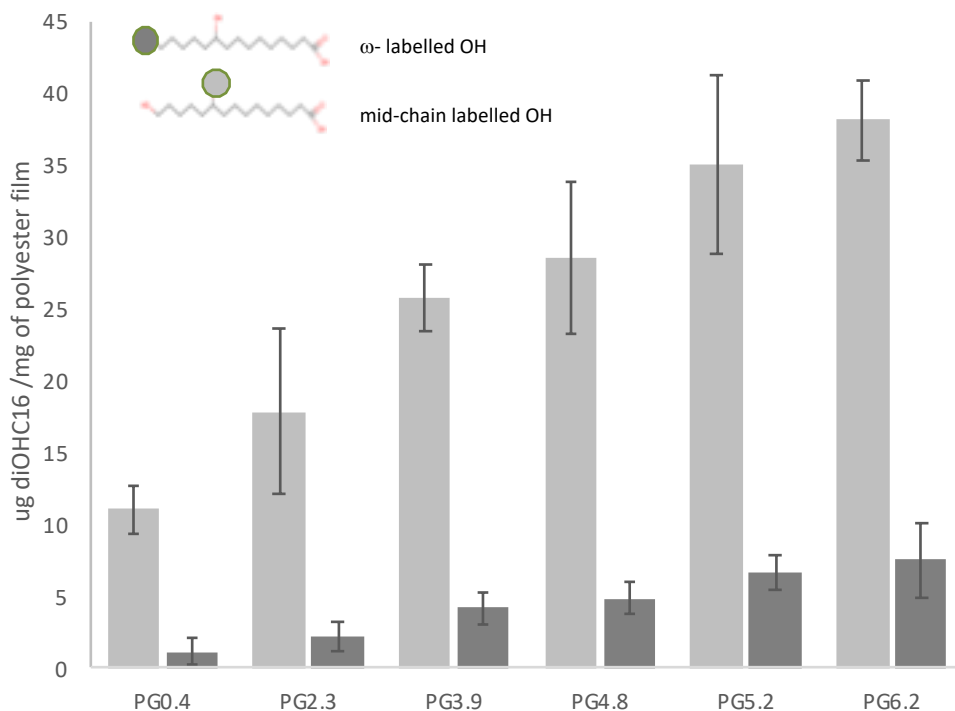


**Figure 3. Relative proportion of free OH groups at the  $\omega$ - and mid-chain position of the the diOHC16 in the co-polyester films.**

Values are means of at least three replicates bars are standard deviations

317

318

319 According to the chemical structure of the diOHC16, both, linear and branched ester bonds, can be  
320 formed in the co-polyesters. After complete depolymerization, the release of diOHC16 containing labeled  
321 OH groups either in  $\omega$ -position or in midchain-position was compared in the different co-polyesters. In  
322 PG0.4, the ratio of labeled mid-chain OH/ $\omega$ -OH labeled in diOHC16 was around 9, which indicates that the  
323 primary OH groups in the  $\omega$ -position were preferentially esterified compared to the OH groups in the  
324 midchain position. This result agrees with the NMR data (**Figure 2B**) and the previous studies of  
325 polycondensation of polyhydroxylated fatty acids (Benitez et al., 2015). A similar ratio was previously

326 reported for tomato fruit cutin (Philippe et al., 2016). Furthermore, taking PG0.4 as a reference, the gradual  
327 introduction of glycerol in the co-polyesters resulted in a gradual increase (up to 3.5-fold) in the labeled  
328 OH groups, in particular in the midchain position. These results indicate that the introduction of glycerol  
329 in the co-polyesters induced a gradual decrease in the esterification of midchain hydroxyl groups involved  
330 in ester bonds and an increase in the linear polymerization scheme within the co-polyesters.

331

### 332 **3.3. Glycerol content modulates the microstructure and thermo-mechanical properties of the** 333 **co-polyesters**

334

335 The thermal properties of all the produced co-polyesters were investigated by DSC on heating from -50°C  
336 to 80°C at 3°C.min<sup>-1</sup>. Characteristic thermograms are superimposed in **Figure 4A**. We checked that the  
337 cooling step at -50°C did not modify the crystallinity of the samples. The thermograms of the co-polyesters  
338 exhibited various events as a function of the composition, i.e., the amount of esterified glycerol in the  
339 samples. From -30°C to 0°C, depending on the glycerol content, the baseline fall was attributed to the glass  
340 transition characterizing the amorphous phase of the co-polyesters. The glass transition temperatures (T<sub>g</sub>),  
341 determined at the midpoint of the baseline fall, were determined for each co-polyester (**Table 1**). The T<sub>g</sub>  
342 value determined for the PG0.4 sample containing only traces of glycerol is -8.7°C, similar to that measured  
343 on polyester catalyst- produced (-7°C) from hydroxy fatty acids extracted from green tomato cutin (Benitez  
344 et al., 2015). Interestingly, the T<sub>g</sub> significantly decreased from -8.7 to -20.4°C with the gradual introduction  
345 of glycerol (up to 6.2% wt.) within the co-polyesters, suggesting that the mobility of the co-polyester chains  
346 increased giving rise to a more relaxed structure. This result is consistent with the observed reticulation  
347 pattern of the co-polyesters (**Figure 3**).

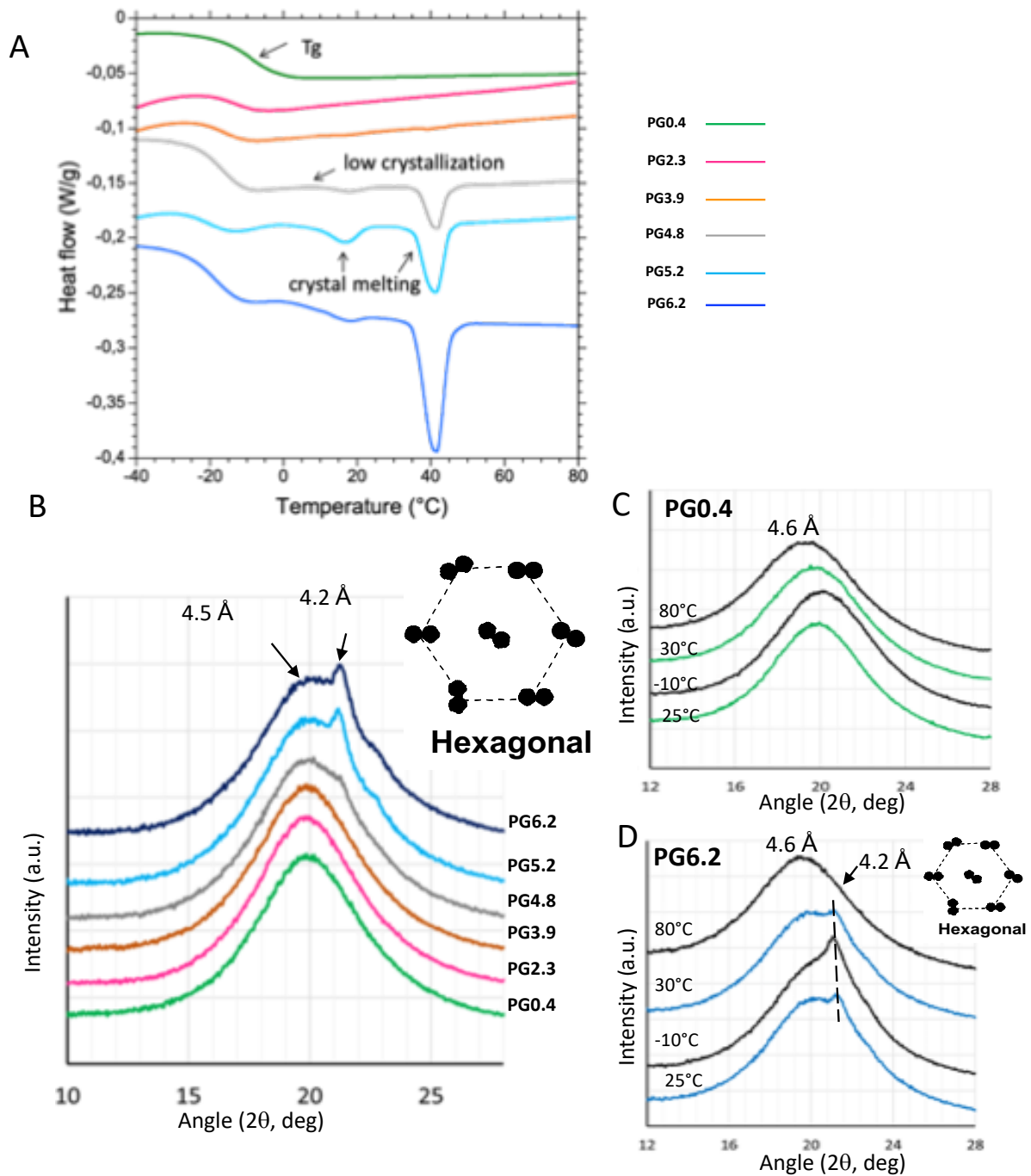


**Figure 4. DSC and XRD analyses of the different cutin-like diOHC16-glycerol co-polyester films**

**A** . DSC thermogram of the different co-polyesters containing increasing level of glycerol from 0.4 % wt (for PG0.4) to 6.2% wt (for PG6.2). **B**, XRD patterns of the different co-polyesters recorded at 25°C., XRD patterns recorded for PG0.4 (**C**) and PG6.2 (**D**) at different temperatures.

348

349 For the co-polyesters containing glycerol amounts lower than 4% wt. (PG0.4, PG2.3, PG3.9), the DSC

350 thermograms recorded on heating did not exhibit thermal events above 0°C (**Figure 4A**). However, for the  
351 co-polyesters containing higher amounts of glycerol (PG4.8, PG5.2, and PG6.2), endothermic events were  
352 recorded and related to the gradual incorporation of glycerol in the materials. Indeed, for these co-  
353 polyesters, two successive endothermic peaks were recorded around 17°C and 40°C. These endotherms  
354 may correspond to structural reorganizations, and/or changes in the physical state of molecules in the co-  
355 polyesters. The second endothermic peak (40°C) exhibits a higher enthalpy than the first, and increases  
356 with the level of glycerol content (**Table 1**).

357 The X-ray diffraction experiments performed at 25°C showed at wide angles a bump centered at  
358  $2\theta=19^\circ$  ( $d=4.5 \text{ \AA}$ ), corresponding to the amorphous state of the co-polyesters (**Figure 4B**). In the co-  
359 polyesters containing at least 5 % wt. of glycerol (PG5.2, PG6.2), a peak at  $2\theta=21.2^\circ$  was recorded (**Figure**  
360 **4B**). This peak corresponds to a repeat distance of  $4.2 \text{ \AA}$  between the acyl chains which is characteristic of  
361 a hexagonal packing of acyl chains. This single peak constitutes the XRD signature of the formation of a  
362 crystalline organization of the linear esterified acyl chains within the co-polyesters containing at least 5%  
363 wt. glycerol. This XRD peak was superimposed to the bump centered at  $4.5 \text{ \AA}$  (**Figure 4B**), which  
364 corresponds to the coexistence of crystalline and amorphous states within the co-polyesters. The presence  
365 of glycerol in the samples, and the esterification occurring between the hydroxyl groups of glycerol (mainly  
366 in *sn-1* and *sn-3* positions) and the carboxyl groups of the fatty acids induced a linear organization of the  
367 chains or the formation of shorter chains. This spatial proximity between the linear and shorter co-  
368 polyester chains may favor short-distance hydrophobic interactions between the acyl chains and result in  
369 a crystalline organization with a hexagonal packing below the melting temperature of the fatty acids. In  
370 absence of glycerol, the reticulation involves the hydroxyl groups both in midchain hydroxyl and  $\omega$ -

371 positions. This prevents short-distance hydrophobic interactions between the linear chains formed by  
372 primary esterification, hence avoiding the formation of a crystalline organization in the co-polyesters.

373 The thermotropic phase behavior of the co-polyesters formed with very low (PG0.4) or high (PG6.2)  
374 amount of glycerol, were investigated by XRD at various temperatures ranging from -10°C to 80°C that  
375 have been selected according to the DSC results (**Figure 4A**). In presence of very low glycerol content  
376 (**Figure 4C**), the amorphous state of the polyester was characterized by a bump of RX diffusion, centered  
377 in a mean value that was affected by the temperature. The increase of temperature induced a shift toward  
378 lower angle values corresponding to higher distances between the acyl chains associated with an increase  
379 in the molecular mobility. In the presence of 6 % wt. of glycerol (**Figure 4D**), the XRD experiments were  
380 conducted at 25°C, then the samples were cooled to -10°C, heated to 30°C (i.e., above the first endotherm)  
381 and then finally to 80°C (i.e., above the second endotherm). The single peak at  $2\theta=21.2^\circ$  (4.2 Å) was  
382 recorded at 25°C, confirming the results previously obtained. Decreasing the temperature to -10°C  
383 increased the intensity of the XRD peak at  $2\theta=21.2^\circ$  related to a hexagonal phase and was interpreted as  
384 an increase in the amount of the crystalline phase formed in the co-polyesters. On heating at 30°C, the  
385 intensity of the XRD decreased. Increasing the temperature at 80°C, i.e., above the second endotherm  
386 recorded by DSC and then above the melting point of the crystalline structures, induced the disappearance  
387 of the XRD peak at  $2\theta=21.2^\circ$  and to the recording of an XRD bump centered at 4.6 Å characteristic of acyl  
388 chains in a melted state. These XRD experiments evidenced the temperature-dependent behavior of the  
389 co-polyester, with the presence of various amounts of hexagonal phase as a function of temperature.

390 The two endotherms revealed successively by DSC correspond to independent packing events of  
391 the molecules both organized in a hexagonal form as revealed by XRD. The different melting temperatures  
392 may correspond to packing of molecules with various compositions, *e.g.* chain length.

393 The thermo-mechanical behavior of all co-polyesters was analyzed by DMTA. **Figure 5A** shows the  
394 plot of the storage modulus ( $E'$ ) and the loss factor  $\tan \delta$  of the co-polyesters. For all samples, the large  
395 peak of  $\tan \delta$  corresponds to the main mechanical relaxation  $\alpha$  which is associated with the calorimetric  
396 glass transition from a glassy to a rubbery state. The relaxation temperature from the glassy to the rubbery  
397 state ( $T_\alpha$ ), determined at the maximum of the  $\tan \delta$  curve, decreases from 8.6°C to 0.2°C when glycerol  
398 content increases (**Table 1**). In agreement with the  $T_g$  values obtained by DSC analyses (**Table 1**) such a  
399 depressor effect of glycerol on  $T_\alpha$  further strengthens the impact of glycerol on the properties of the cutin-

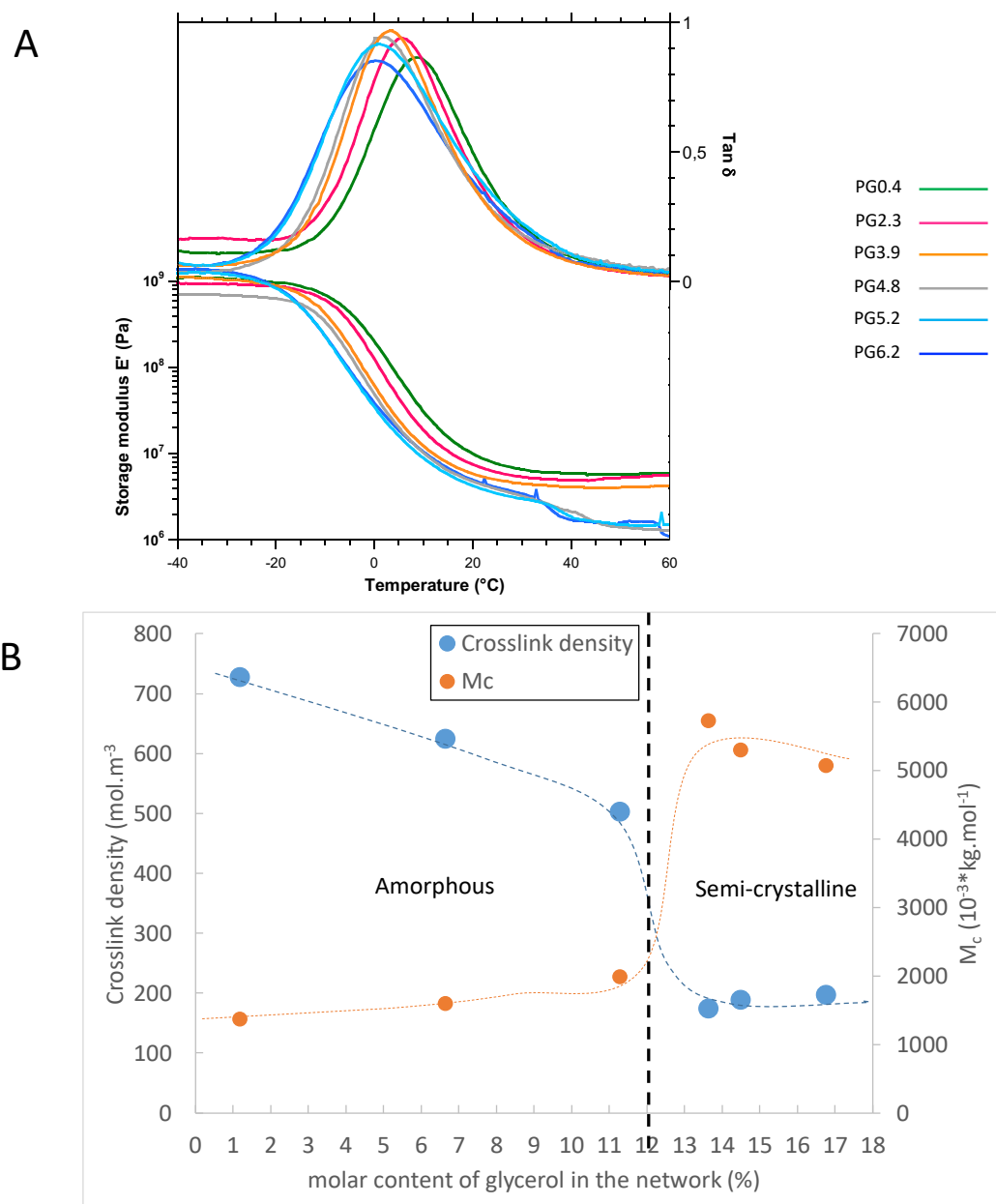


**Figure 5 – DMA analysis of the cutin-like diOHC16-glycerol co-polyesters**

A – Plot of the storage modulus ( $E'$ ) and the loss factor  $\tan \delta$  of the co-polyesters with different level of esterified glycerol content.

B- Evolution of the crosslink density and the average mass between crosslinks as a function of the molar content of glycerol in the network. Dashed lines are just guides for the eyes.

402 A second event appears on storage modulus which slightly falls in the temperature range 30-40°C  
403 for the composition containing more than 4% (wt.) of glycerol (PG4.8, PG5.2, PG6.2) (**Figure 5A**). This  
404 transition is attributed to the melting of the crystalline phase according to DSC and XRD results (**Figure 4**).  
405 Finally, the plateau of storage modulus is reached at about 50°C with a value which decreases from 5.867  
406 MPa to 1.589 MPa when glycerol content increases from 0.4 to 6% wt. (**Table 1**).  
407 These values are typical of rubber elasticity suggesting an elastomeric behavior of the co-polyesters. This  
408 was confirmed by the tensile tests performed at room temperature. The tensile strength, strain at break  
409 and, Young Modulus are reported in **Table1**, and the characteristic curves are plotted in **Figure 6**.

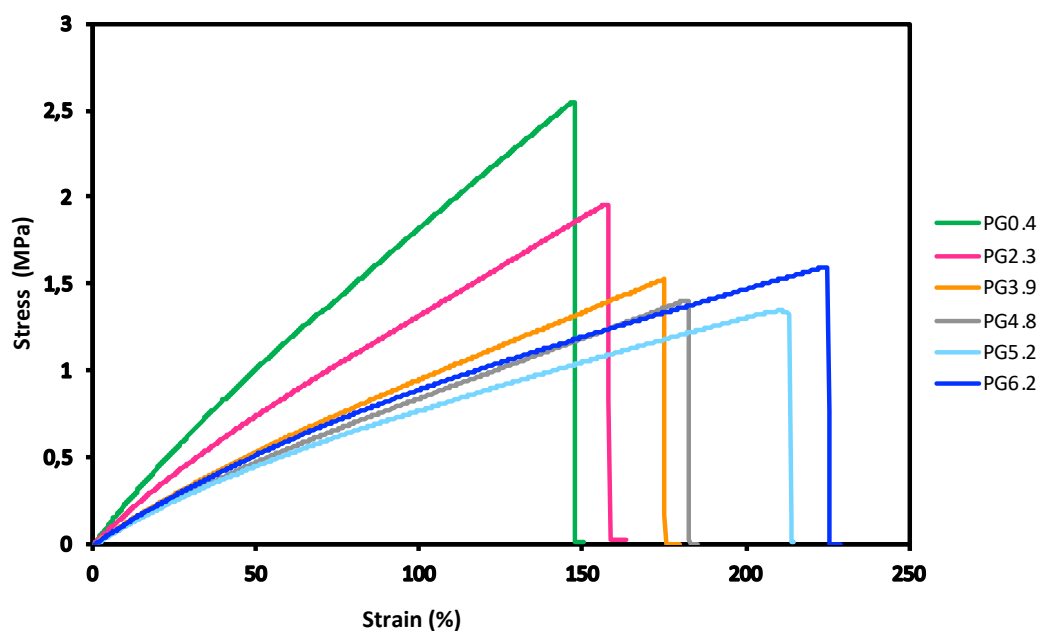


Figure 6- Typical Stress-strain curves of the cutin-like diOHC16-glycerol co-polyester films from 0.4 % wt. for PG0.4 to 6.2% wt. for PG6.2

410  
411 All films, either with low or high glycerol contents, show a quasi-linear and reversible stress-strain  
412 behavior with high elongation at break (> 100%) comparable to synthetic elastomers. It is striking that after

413 breakage, the dogbone tensile test specimens show a complete elastomeric recovery of their initial shape  
414 (Supplemental Figure 2). The mechanical properties of the PG0.4 are comparable to those previously  
415 described for other polyhydroxylated fatty acid-based polyesters (Benitez et al., 2015; Benítez et al., 2015).  
416 Moreover, our present data show that the mechanical properties were strongly modified by the gradual  
417 introduction of glycerol in the co-polyesters which resulted in a decrease in the Young modulus (from 2.29  
418 to 1.19 MPa), as well as in the stress at break (from 2.1 to 1.5 MPa). Surprisingly, higher glycerol of 6%  
419 induces a slight increase of tensile strength simultaneous to the increase of strain at break. It is certainly  
420 due to the crystallinity evidenced by calorimetry and XRD measurements (Figure 4).

421 The most striking observation is the increase in strain at break from 124% to 217 % (for PG0.4 and  
422 PG6.2 respectively) induced by the esterified glycerol in the co-polyesters (**Table1, Figure 6**). This  
423 elongation value is comparable to some synthetic rubber such as ethylene-propylene-diene or polysulfide-  
424 butadiene rubbers (Shanks and Kong, 2013). This strain at break induced by a higher glycerol/hydroxy fatty  
425 acid ratio fully fits the CUS1 tomato phenotype which is affected in cutin deposition (Philippe et al., 2016).  
426 Importantly, the CUS1 tomato cutin polyester exhibited a fivefold increase in the glycerol ratio (vs hydroxy  
427 fatty acids), which probably account for the increase in its extensibility and the absence of cracks observed  
428 on the CUS1 fruits, regardless that their cuticle density shows a threefold reduction (Girard et al., 2012).

429  
430 Since our co-polyesters behave like elastomers displaying rubber elasticity, the Flory theory (Flory,  
431 1953) may bring information about the macromolecular structure of the networks (Tran et al., 2018).  
432 Accordingly, the crosslink density  $\nu$  (mole.m<sup>-3</sup>) is given by:

433 
$$\nu = \frac{E}{3RT} \quad (\text{equation 2})$$

434 Where: R is the gas constant 8.32 J.mol<sup>-1</sup>.K<sup>-1</sup>, T is the temperature in Kelvin, and E the elastic modulus at  
 435 small deformation. This model assumes that the material is amorphous and consequently, we will use the  
 436 plateau storage modulus values measured in DMTA at 50°C (T = 323 K, that is to say above the melting  
 437 point of the semi-crystalline samples.).

438 Therefore, the average molecular mass  $M_c$  (kg.mol<sup>-1</sup>) of elastically active chains between crosslinks is:

439 
$$M_c = \frac{3RT\rho}{E}$$
 (equation 3)

440 Where:  $\rho$  is the density of the material in Kg.m<sup>-3</sup>. The density of the co-polyesters at 50°C could not be  
 441 measured. As a first approximation, we considered a constant density  $\rho = 1000$  kg.m<sup>3</sup> for the calculations  
 442 reported in **Table 2 and Figure 5B**.

	n	$M_c$ (g/mol)	$M_c/M_0$	Esterified molar glycerol content *
	(mol.m <sup>-3</sup> )	(10 <sup>-3</sup> kg.mol <sup>-1</sup> )	-	mol %
<b>PG 0.4</b>	728	1374	5.1	1.2
<b>PG 2.3</b>	625	1601	5.9	6.64
<b>PG 3.9</b>	503	1987	7.4	11.3
<b>PG 4.8</b>	175	5726	21.2	13.6
<b>PG 5.2</b>	189	5301	19.6	14.5
<b>PG 6.2</b>	197	5074	18.8	16.8

\* the molar content of glycerol in the networks given by

$$\text{esterified Glycerol (mol\%)} = \frac{\text{esterified glycerol w\%}}{M_{\text{glycerol}}} \div \left( \frac{\text{esterified glycerol w\%}}{M_{\text{glycerol}}} + \frac{(100 - \text{free glycerol w\%} - \text{esterified glycerol w\%})}{M_{\text{diol16}}} \right)$$

Table 2 : Macromolecular structure of the network predicted by the Flory theory

443  
 444 PG0.4, PG2.3, and PG3.9 show the largest crosslink density values in the range of 500- to 730 mol.m<sup>-3</sup>  
 445 associated with small values of  $M_c$  in the 1300-2000 g.mol<sup>-1</sup> range. Concurrently, much lower values of  $\nu$   
 446 (175 to 200 mol.m<sup>-3</sup>) are obtained for samples PG4.8, PG5.2, and PG6.2, with higher values of  $M_c$  in the  
 447 5000-5700 g.mol<sup>-1</sup> range.

448 In a first approximation, the number of polymerized diOHC16 repeating units between crosslinks  
449 can be estimated by dividing these values of  $M_c$  by a repeating unit mass  $M_o = 270 \text{ g}\cdot\text{mol}^{-1}$  (this value  
450 assumes that elastically active chains consist essentially of polymerized diOHC16 monomer units in which  
451 only 1 acid and 1 hydroxyl group have reacted.)

452 The values of the ratio  $M_c/M_o$  calculated in **Table 2** suggest that for samples PG0.4, PG2.3, and  
453 PG3.9 the number of polymerized diOHC16 repeating units should range from 5 to 7, while 19 to 21  
454 repeating units are predicted for samples PG4.8, PG5.2, and PG6.2. For the latter, a few glycerol units are  
455 probably also present in the elastically active chains. Anyhow, such a loosening of the network induced by  
456 the gradual introduction of the glycerol is in full accordance with the increase in the labeling of free OH  
457 groups within the co-polyesters (**Figure 3**).

458 Besides, the plot of  $v$  and  $M_c$  as a function of this molar content of glycerol chemically bound to the  
459 network is shown in Figure 5B. A sharp transition from dense amorphous networks (PG0.4, PG2.3, and  
460 PG3.9) to loose semi-crystalline networks (PG4.8, PG5.2, and PG6.2) seems to take place around a  
461 threshold value of 12 mol% of glycerol.

462 The development of crystallinity for higher glycerol contents may be ascribed to the flexibility of  
463 the long-chain segments between two crosslinks which become able to fold into crystallites, while at lower  
464 glycerol content the shorter chains remain amorphous.

465

466

467 **3.4. Glycerol can modify the barrier properties of the co-polyesters and their interaction with**  
468 **bacterial cells**

469 Water permeance and oxygen barrier properties of the co-polyesters were analyzed. All the produced co-  
470 polyesters showed low water vapor permeance properties (**Figure 7A**) around  $10^{-9}$  m.s<sup>-1</sup>, in the same range  
471 as the plant cuticle permeance and some synthetic membrane, such as 3µm parafilm or 3µm polyethylene  
472 (Valeska Zeisler-Diehl et al., 2017). The introduction of esterified glycerol and the associated modification  
473 of the branching of the co-polyesters induced a slight, but statistically not significant, increase in the water  
474 vapor permeability of the co-polyesters. This result is consistent with our previous data showing that a  
475 modification of the polymerization index did not significantly impact the water permeance of tomato  
476 cutins (Philippe et al, 2016).

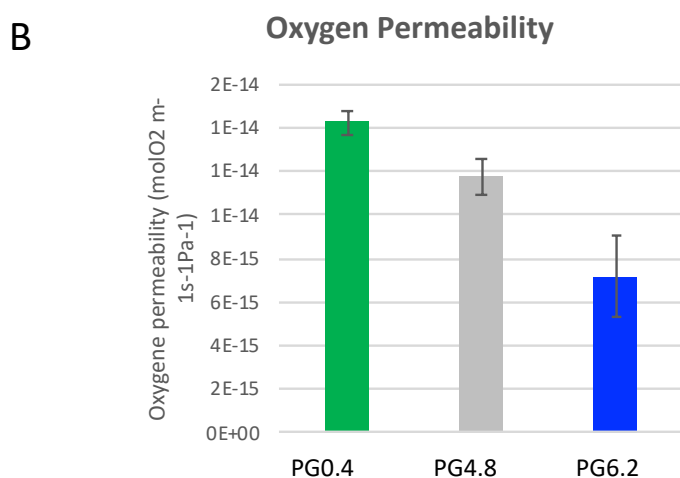
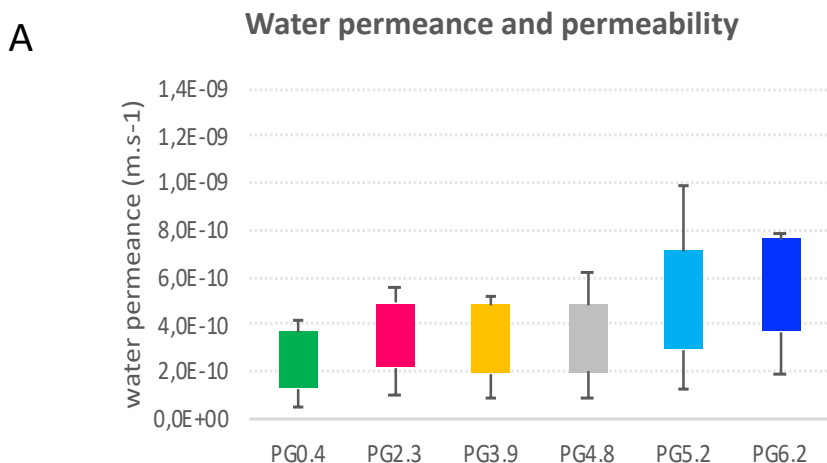


**Figure 7- Barrier properties of the cutin-like co-polyesters**

Water permeance (A) and Oxygen (B) barrier properties of the cutin-like diOHC16-glycerol co-polyesters containing increasing level of glycerol (0.4 %wt for PG0.4 to 6.2% wt for PG6.2 )

477

478 The oxygen permeability of the cutin-derived co-polyesters ranged between 0.7 and 1.4 x 10<sup>-14</sup> mol  
 479 m<sup>-1</sup>s<sup>-1</sup>Pa<sup>-1</sup> (Figure 7B). These values are in the same order of magnitude as synthetic polymers commonly  
 480 used for food packaging such as low-density polyethylene (0.1-0.2 x 10<sup>-14</sup> mol.m<sup>-1</sup>.s<sup>-1</sup>.Pa<sup>-1</sup>) (Durmuş et al.,  
 481 2007; Matar et al., 2018; Motedayen et al., 2019). These values are also comparable to polylactic acid  
 482 (PLA), a bio-based polyester, for which oxygen permeability values ranging between 1x10<sup>-16</sup> and 1x10<sup>-14</sup>  
 483 mol. m<sup>-1</sup>.s<sup>-1</sup>.Pa<sup>-1</sup> have been reported (Lehermeier et al., 2001; Mahmoodi et al., 2019; Palai et al., 2019).

484 Other polyesters such as fossil-based polyethylene terephthalate, or microbial synthesized  
485 polyhydroxyalkanoates (PHAs) have considerably higher barrier properties with oxygen permeability in the  
486 order of  $1 \times 10^{-17} \text{ mol m}^{-1} \text{ s}^{-1} \text{ Pa}^{-1}$  (Ambrosio-Martin et al., 2016; Crétois et al., 2014).

487 Interestingly, increasing the ratio of esterified glycerol in the co-polyesters improved the oxygen  
488 barrier properties of the films by reducing oxygen permeability by half (**Figure 7B**). This is probably  
489 associated with the increase of crystallinity, as observed for other elastomers (Wang et al., 2012) reducing  
490 the motion needed for oxygen diffusion.

491 Finally, the antibacterial activity of the co-polyesters containing the lowest and the highest levels  
492 of esterified glycerol (PG0.4 and PG6.2) was assessed on *E. coli* and *S. aureus*. After exposure to the co-  
493 polyester films, no labeling of dead cells was revealed (**Figure 8A**), which indicates that the co-polyesters  
494 were devoid of bactericidal properties regardless of the glycerol content. This result contrasts with the  
495 biocide activity that was demonstrated with acyl glycerol esters of hydroxy fatty acids (Correia et al., 2020)  
496 or with films formed by self-assembly of these esters (Ferreira et al., 2014; Garcia et al., 2010) extracted  
497 by an ionic liquid catalyst from suberin, another hydrophobic plant polyesters.

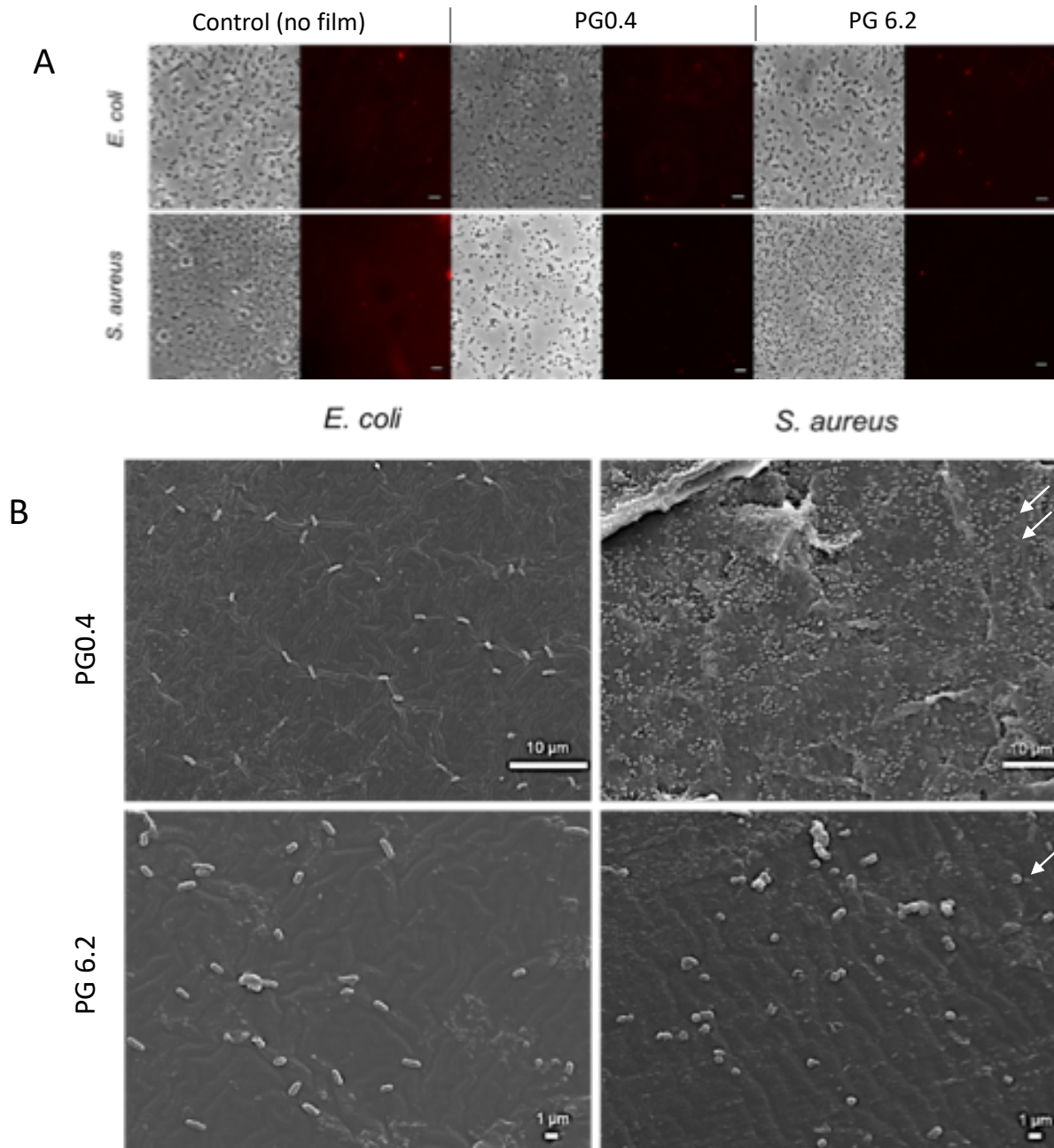


**Figure 8.** Microscopy imaging of the cutin-like co-polyesters PG0.4 and PG6.2 after incubation with *E. coli* and *S. aureus*.

**A.** Co-polyesters films activity against *E. coli* and *S. aureus*. Following exposure of bacteria to films pieces their morphology and viability were visualized by phase-contrast and fluorescence microscopy using Texas Red filter (dead cells are revealed by red fluorescence due to propidium iodide labelling), respectively. Controls was conducted without films. The scale bar in all images is 5 $\mu$ m.

**B.** Cells adherent onto the surface of the cutin co-polyester films were observed by SEM microscopy. No differences were noticed in the numbers of adherent *E. coli* cells in either co-polyester films. Conversely, the number of *S. aureus* adherent cells (ex under arrows) are significantly higher in the PG0.4 co-polyester compared to the PG6.2. The scale bar in all images is shown at the bottom.

499            Since the co-polyesters are devoid of bactericidal capacity, we further analyzed the films' surface  
500 following their incubation with bacteria (**Figure 8 B**). For either co-polyester, the numbers of adherent *E.*  
501 *coli* cells were low and comparable. Remarkably over the surface of the PG0.4 co-polyester, *S. aureus*  
502 formed a compacted biofilm whereas PG6.2 hinder significantly the adhesion of this bacteria species. This  
503 result demonstrates that increased glycerol levels in the cutin-inspired co-polyesters lead to a significant  
504 reduction of bacterial fouling. (**Figure 8 B**). The observed differences between the two bacteria species  
505 might be due to the electronegativity of the cells surface that is higher in *E. coli* than *S. aureus*, regardless  
506 that their different morphologies and surface roughness (rods and cocci, respectively) may greatly  
507 influence their adhesion in the conditions used here. This observation, supported by the structural,  
508 thermal, and mechanical analyses, suggests that glycerol esterification altered the smoothness of the films'  
509 surface as well as their surface charge. One important finding is that by increasing further the glycerol  
510 levels in the cutin co-polyesters their anti-biofouling properties can be potentiated.

511

512

#### 513        **4. Conclusions**

514            We report in this work, the production of glycerol/hydroxy fatty acid co-polyesters by a catalyst-  
515 and solvent-free polycondensation process. Glycerol and hydroxy fatty acids are biosourced molecules  
516 from by-products and wastes produced by the oilseed and tomato processing industries, respectively.

517            These co-polyesters elastomers obtained are 100% biobased and bioinspired by the cutin polymer of plant  
518 cuticles, which is also composed of hydroxy-fatty acids and glycerol. Drawing on our previous studies on  
519 tomato fruit cuticle, we gradually increased the glycerol content while remaining in a concentration range  
520 observed in most plant cuticles. The co-polyesters obtained are insoluble and displayed tensile mechanical

521 behavior comparable to that of some synthetic elastomers. By adjusting the level of esterified glycerol,  
522 we induced modifications of the reticulation pattern which was associated with variation in chain mobility  
523 and extensibility. Glycerol also induced the loosening of the elastically active chain network and the  
524 formation of crystalline domains. These modifications were associated with variations in the tensile  
525 mechanical and barrier properties of the co-polyesters as well as the adhesion of microorganisms.

526 The exact macromolecular structure of the co-polyesters probably involves not only glycerol and  
527 diOHC16 but also minor components present in the fatty acid extract. The elucidation of the role in the  
528 reaction scheme will be the subject of future work. Indeed, these hydroxy fatty acid/glycerol co-polyesters  
529 provide excellent templates to further delineate the relationships between the complex molecular and  
530 macromolecular architecture and the functional properties of plant cuticular barriers. This bioinspired  
531 approach also allows developing green polymer composites adapted to specific applications for food,  
532 packaging industry, or as an antifouling natural product. Furthermore, increasing the contents of glycerol  
533 led to available free hydroxyl groups for grafting and covalent substitutions for tailored functionalization,  
534 opening new routes for high-value applications (e.g., in the medical sector).

535

### 536 **Figure Caption**

537 **Figure 1 – Solvent- and catalyze-free polycondensation of tomato cutin extract and glycerol**

538 **Figure 2 – ATR-FTIR and NMR spectra of the cutin-like polyesters films**

539 **A** . ATR-FTIR spectra of hydroxy fatty acid (diOHC16) extracted from tomato cutin and the corresponding  
540 polymers with high (PG6.2) or low (PG0.4) glycerol. In the inset, the magnification of the C=O stretching  
541 bands at  $1715\text{ cm}^{-1}$  and  $1733\text{ cm}^{-1}$  are assigned to the ester group, involved or not in hydrogen bonds,  
542 respectively, whereas the vibration at  $1703\text{ cm}^{-1}$  is assigned to the carboxylic group.

543 **B. Solid-State  $^{13}\text{C}$  CP-MAS NMR spectra of the polymers**

544

545 **Figure 3- Relative proportion of free OH groups at the  $\omega$ - and mid-chain position of the diOHC16 in the co-**  
546 **polyester films.**

547 Values are means of at least three replicates bars are standard deviations

548

549 **Figure 4- DSC and XRD analyses of the different cutin-like diOHC16-glycerol co-polyester films**

550 **A**, DSC thermogram of the different co-polyesters containing increasing levels of glycerol from 0.4 % wt  
551 (for PG0.4) to 6.2% wt (for PG6.2). **B**, XRD patterns of the different co-polyesters recorded at 25°C. XRD  
552 patterns for PG0.4 (**C**) and PG6.2 (**D**) recorded at different temperatures.

553

554 **Figure 5- DMA analysis of the cutin-like diOHC16-glycerol co-polyesters**

555 **A** – Plot of the storage modulus ( $E'$ ) and the loss factor  $\tan\delta$  of the co-polyesters with different levels of  
556 esterified glycerol content.

557 **B**- Evolution of the crosslink density and the average mass between crosslinks as a function of the molar  
558 content of glycerol in the network. Dashed lines are just a guide for the eye.

559

560 **Figure 6- Typical Stress-strain curves of the cutin-like diOHC16-glycerol co-polyester films from 0.4 % wt. for PG0.4**  
561 **to 6.2% wt. for PG6.2**

562

563 **Figure 7- Barrier properties of the cutin-like co-polyesters**

564 Water permeance (A) and oxygen (B) barrier properties of the cutin-like diOHC16-glycerol co-polyesters  
565 containing increasing levels of glycerol (0.4 %wt for PG0.4 to 6.2% wt for PG6.2)

566

567 **Figure 8- Microscopy imaging of the cutin-like co-polyesters PG0.4 and PG6.2 after incubation with *E. coli* and *S.***  
568 ***aureus*.**

569 **A.** Co-polyesters films activity against *E. coli* and *S. aureus*. Following exposure of bacteria to film pieces,  
570 their morphology and viability were visualized by phase-contrast and fluorescence microscopy using Texas  
571 Red filter (dead cells are revealed by red fluorescence due to propidium iodide labelling), respectively.  
572 Controls were conducted without films. The scale bar in all images is 5 $\mu$ m.

573 **B.** Cells adherent onto the surface of the cutin co-polyester films were observed by SEM microscopy. No  
574 differences were noticed in the numbers of adherent *E. coli* cells in either co-polyester films. Conversely,  
575 the number of *S. aureus* adherent cells (ex under arrows) are significantly higher in the PG0.4 co-polyester  
576 compared to the PG6.2. The scale bar in all images is shown at the bottom.

577

578 **Supplemental Figure 1- Composition and characterization of the cutin monomer extracted from tomato cutin**  
579 **from industrial tomato peels**

580 A. Cutin monomer composition. Values are means (standard deviation) of three experiments. B. FTIR  
581 spectrum. C. UV spectrum

582

583 **Supplemental Figure 2- Elastomeric recovery cutin-inspired polyesters.**

584 On the left, an image of the elastomeric sample (PG0.4) before and after a mechanical test (right) showing  
585 its total shape recovery

586

## 587 **Acknowledgment**

588 This work was supported by an INRAE Transfer grant (ELASTOMAT project) and the INRAE

589 TRANSFORM department. RR is grateful to FCT funding for his Ph.D. scholarship (SFRH-BD-110467-2015).

590 The authors thank André Lelion for his technical assistance.

## 591 **References**

- 592 Aleixandre-Tudo, J.L., du Toit, W., 2018. The role of UV-visible spectroscopy for phenolic compounds  
593 quantification in winemaking, in: Solis-Oviedo, R.L., dela Cruz Pech-Canul, A. (Eds.), *Frontiers*  
594 *and new trends in the science of fermented food and beverages*.  
595 <https://doi.org/DOI:10.5772/intechopen.79550>
- 596 Ambrosio-Martin, J., Fabra, M.J., López-Rubio, A., Gorrasi, G., Sorrentino, A., Lagaron, J.M., 2016.  
597 Assessment of ball milling as a compounding technique to develop nanocomposites of poly(3-  
598 hydroxybutyrate-co-3-hydroxyvalerate) and bacterial cellulose nanowhiskers. *J. Polym. Environ.*  
599 *24*, 241-254. <https://doi.org/10.1007/s10924-016-0767-6>
- 600 Barker, J.C., 1988. Russeting (cuticle cracking) in glasshouse tomatoes in relation to fruit growth. *J.*  
601 *Hortic. Sci.* *63*, 459-463. <https://doi.org/10.1080/14620316.1988.11515879>
- 602 Benítez, J.J., Castillo, P.M., Del Río, J.C., León-Camacho, M., Domínguez, E., Heredia, A., Guzmán-  
603 Puyol, S., Athanassiou, A., Heredia-Guerrero, J.A., 2018. Valorization of tomato processing by-  
604 products: fatty acid extraction and production of bio-based materials. *Materials (Basel)*  
605 *11*. <https://doi.org/10.3390/ma11112211>
- 606 Benitez, J.J., Heredia-Guerrero, J.A., Guzman-Puyol, S., Barthel, M.J., Dominguez, E., Heredia, A., 2015.  
607 Polyhydroxyester films obtained by non-catalyzed melt-polycondensation of natural occurring  
608 fatty polyhydroxyacids. *Front. Mater.* *2*, 10. <https://doi.org/10.3389/fmats.2015.00059>
- 609 Benítez, J.J., Heredia-Guerrero, J.A., Guzmán-Puyol, S., Domínguez, E., Heredia, A., 2015. Long-chain  
610 polyhydroxyesters from natural occurring aleuritic acid as potential material for food packaging.  
611 *Soft Mater.* *13*, 5-11. <https://doi.org/10.1080/1539445X.2014.993476>
- 612 Cogognigni, I., Montanari, A., de la Torre Carreras, R., Cardoso Bernet Montserrat, G., 2014. Extraction  
613 method of a polyester polymer or cutin from the wasted tomato peels and polyester polymer so  
614 extracted
- 615 Correia, V.G., Bento, A., Pais, J., Rodrigues, R., Haliński, Ł.P., Frydrych, M., Greenhalgh, A., Stepnowski,  
616 P., Vollrath, F., King, A.W.T., Silva Pereira, C., 2020. The molecular structure and  
617 multifunctionality of the cryptic plant polymer suberin. *Materials Today Bio* *5*,  
618 100039. <https://doi.org/10.1016/j.mtbio.2019.100039>
- 619 Crétois, R., Follain, N., Dargent, E., Soulestin, J., Bourbigot, S., Marais, S., Lebrun, L., 2014.  
620 Microstructure and barrier properties of PHBV/organoclays bionanocomposites. *J. Membrane*  
621 *Sci.* *467*, 56-66. <https://doi.org/10.1016/j.memsci.2014.05.015>
- 622 Durmuş, A., Woo, M., Kaşgöz, A., Macosko, C.W., Tsapatsis, M., 2007. Intercalated linear low density  
623 polyethylene (LLDPE)/clay nanocomposites prepared with oxidized polyethylene as a new type  
624 compatibilizer: Structural, mechanical and barrier properties. *Eur. Polym. J.* *43*, 3737-  
625 3749. <https://doi.org/10.1016/j.eurpolymj.2007.06.019>
- 626 Fameau, A.-L., Gaillard, C., Marion, D., Bakan, B., 2013. Interfacial properties of functionalized  
627 assemblies of hydroxy-fatty acid salts isolated from fruit tomato peels. *Green Chem.* *15*, 341-  
628 346. <https://doi.org/10.1039/C2GC36677K>

629 Feast, W.J., Stainton, N.M., 1995. Synthesis, structure and properties of some hyperbranched polyesters.  
630 Journal of Materials Chemistry 5, 405-411.<https://doi.org/10.1039/JM9950500405>

631 Ferreira, R., Garcia, H., Sousa, A.F., Guerreiro, M., Duarte, F.J.S., Freire, C.S.R., Calhorda, M.J.,  
632 Silvestre, A.J.D., Kunz, W., Rebelo, L.P.N., Silva Pereira, C., 2014. Unveiling the dual role of the  
633 cholinium hexanoate ionic liquid as solvent and catalyst in suberin depolymerisation. RSC  
634 Advances 4, 2993-3002.<https://doi.org/10.1039/C3RA45910A>

635 Fich, E.A., Segerson, N.A., Rose, J.K., 2016. The plant polyester cutin: biosynthesis, structure, and  
636 biological roles. Annu. Rev. Plant Biol. 67, 207-233.<https://doi.org/10.1146/annurev-arplant-043015-111929>

637 Flory, J.P., 1953. Elasticity of rubber, Principles of Polymer Chemistry, Ithaca, N.Y. : Cornell University  
638 Press ed. <https://doi.org/DOI:10.1126/science.119.3095.555-a>.

640 Fritsch, C., Staebler, A., Happel, A., Cubero Márquez, M.A., Aguiló-Aguayo, I., Abadias, M., Gallur, M.,  
641 Cigognini, I.M., Montanari, A., López, M.J., Suárez-Estrella, F., Brunton, N., Luengo, E., Sisti, L.,  
642 Ferri, M., Belotti, G., 2017. Processing, valorization and application of bio-waste derived  
643 compounds from potato, tomato, olive and cereals: A Review. 9,  
644 1492.<https://doi.org/doi:10.3390/su9081492>

645 Garcia, H., Ferreira, R., Petkovic, M., Ferguson, J.L., Leitão, M.C., Gunaratne, H.Q.N., Seddon, K.R.,  
646 Rebelo, L.P.N., Silva Pereira, C., 2010. Dissolution of cork biopolymers in biocompatible ionic  
647 liquids. Green Chem. 12, 367-369.<https://doi.org/10.1039/B922553F>

648 Girard, A.L., Mounet, F., Lemaire-Chamley, M., Gaillard, C., Elmorjani, K., Vivancos, J., Runavot, J.L.,  
649 Quemener, B., Petit, J., Germain, V., Rothan, C., Marion, D., Bakan, B., 2012. Tomato GDGL1 is  
650 required for cutin deposition in the fruit cuticle. Plant Cell 24, 3119-  
651 3134.<https://doi.org/10.1105/tpc.112.101055>

652 Graça, J., Schreiber, L., Rodrigues, J., Pereira, H., 2002. Glycerol and glyceryl esters of omega-  
653 hydroxyacids in cutins. Phytochemistry 61, 205-215.[https://doi.org/10.1016/s0031-9422\(02\)00212-1](https://doi.org/10.1016/s0031-9422(02)00212-1)

654 Heredia-Guerrero, J.A., Benítez, J.J., Domínguez, E., Bayer, I.S., Cingolani, R., Athanassiou, A., Heredia,  
655 A., 2014. Infrared and Raman spectroscopic features of plant cuticles: a review. Front. Plant Sci.  
656 5, 305.<https://doi.org/10.3389/fpls.2014.00305>

657 Heredia-Guerrero, J.A., Heredia, A., Dominguez, E., Cingolani, R., Bayer, I.S., Athanassiou, A., Benitez,  
658 J.J., 2017. Cutin from agro-waste as a raw material for the production of bioplastics. J. Exp. Bot.  
659 68, 5401-5410.<https://doi.org/10.1093/jxb/erx272>

660 Herrera, F., Pulgarin, C., Nadtochenko, V., Kiwi, J., 1998. Accelerated photo-oxidation of concentrated p-  
661 coumaric acid in homogeneous solution. Mechanistic studies, intermediates and precursors  
662 formed in the dark. Appl. Catal. B-Environ. 17, 141-156.[https://doi.org/10.1016/S0926-3373\(98\)00008-3](https://doi.org/10.1016/S0926-3373(98)00008-3)

663 Lehermeier, H.J., Dorgan, J.R., Way, J.D., 2001. Gas permeation properties of poly(lactic acid). J.  
664 Membrane Sci. 190, 243-251.[https://doi.org/10.1016/S0376-7388\(01\)00446-X](https://doi.org/10.1016/S0376-7388(01)00446-X)

665 Mahmoodi, A., Ghodrati, S., Khorasani, M., 2019. High-strength, low-permeable, and light-protective  
666 nanocomposite films based on a hybrid nanopigment and biodegradable PLA for food packaging  
667 applications. ACS Omega 4, 14947-14954.<https://doi.org/10.1021/acsomega.9b01731>

668 Matar, C., Gaucel, S., Gontard, N., Guilbert, S., Guillard, V., 2018. Predicting shelf life gain of fresh  
669 strawberries 'Charlotte cv' in modified atmosphere packaging. Postharvest Biol. Tec. 142, 28-  
670 38.<https://doi.org/10.1016/j.postharvbio.2018.03.002>

671 Motedayen, A.A., Rezaeigolestani, M., Guillaume, C., Guillard, V., Gontard, N., 2019. Gas barrier  
672 enhancement of uncharged apolar polymeric films by self-assembling stratified nano-composite  
673 films. RSC Advances 9, 10938-10947.<https://doi.org/10.1039/C9RA01109A>

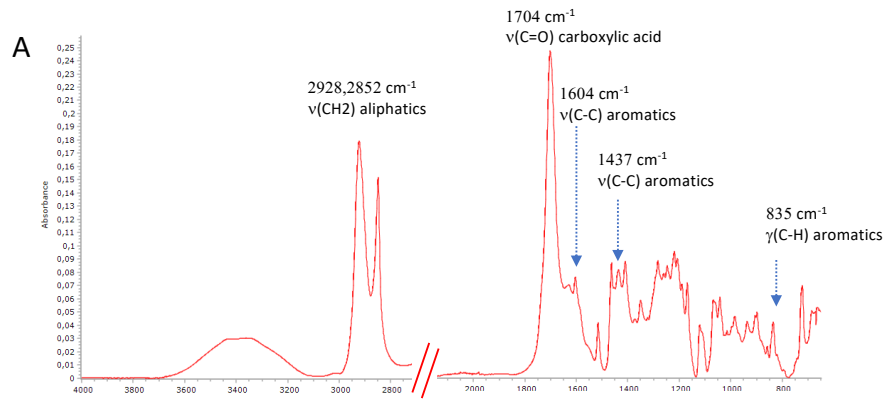
674 Nawrath, C., 2006. Unraveling the complex network of cuticular structure and function. Curr. Opin. Plant  
675 Biol. 9, 281-287.<https://doi.org/10.1016/j.pbi.2006.03.001>

- 678 Palai, B., Biswal, M., Mohanty, S., Nayak, S.K., 2019. In situ reactive compatibilization of polylactic acid  
679 (PLA) and thermoplastic starch (TPS) blends; synthesis and evaluation of extrusion blown films  
680 thereof. *Ind. Crop Prod.* 141, 111748. <https://doi.org/10.1016/j.indcrop.2019.111748>
- 681 Philippe, G., Gaillard, C., Petit, J., Geneix, N., Dalgalarrodo, M., Bres, C., Mauxion, J.P., Franke, R.,  
682 Rothan, C., Schreiber, L., Marion, D., Bakan, B., 2016. Ester cross-link profiling of the cutin  
683 polymer of Wild-Type and cutin synthase tomato mutants highlights different mechanisms of  
684 polymerization. *Plant Physiol.* 170, 807-820. <https://doi.org/10.1104/pp.15.01620>
- 685 Philippe, G., Geneix, N., Petit, J., Guillon, F., Sandt, C., Rothan, C., Lahaye, M., Marion, D., Bakan, B.,  
686 2020. Assembly of tomato fruit cuticles: a cross-talk between the cutin polyester and cell wall  
687 polysaccharides. *New Phytol.* 226, 809-822. <https://doi.org/10.1111/nph.16402>
- 688 Quispe, C.A.G., Coronado, C.J.R., Carvalho Jr, J.A., 2013. Glycerol: production, consumption, prices,  
689 characterization and new trends in combustion. *Renew. Sust. Energ. Rev.* 27, 475-  
690 493. <https://doi.org/10.1016/j.rser.2013.06.017>
- 691 Schreiber L, J. S.n., 2009. Water permeability, Water and solute permeability of plant cuticles. Springer  
692 Berlin Heidelberg, Berlin, Heidelberg, pp. 61-123. <https://doi.org/DOI:10.1007/978-3-540-68945-4>  
693 4
- 694 Shanks, R.A., Kong, I., 2013. General purpose elastomers: structure, chemistry, physics and  
695 performance, in: Visakh, P.M., Thomas, S., Chandra, A.K., Mathew, A.P. (Eds.), *Advances in*  
696 *Elastomers I: Blends and Interpenetrating Networks*. Springer Berlin Heidelberg, Berlin,  
697 Heidelberg, pp. 11-45. [https://doi.org/10.1007/978-3-642-20925-3\\_2](https://doi.org/10.1007/978-3-642-20925-3_2)
- 698 Shen, Y., Xu, Z., 2013. An improved GC-MS method in determining glycerol in different types of biological  
699 samples. *J. Chromatogr. B* 930, 36-40. <https://doi.org/10.1016/j.jchromb.2013.04.034>
- 700 Tedeschi, G., Benitez, J.J., Ceseracciu, L., Dastmalchi, K., Itin, B., Stark, R.E., Heredia, A., Athanassiou,  
701 A., Heredia-Guerrero, J.A., 2018. Sustainable fabrication of plant cuticle-like packaging films  
702 from tomato pomace agro-waste, beeswax, and alginate. *ACS Sustain. Chem. Eng.* 6, 14955-  
703 14966. <https://doi.org/10.1021/acssuschemeng.8b03450>
- 704 Testud, B., Pintori, D., Grau, E., Taton, D., Cramail, H., 2017. Hyperbranched polyesters by  
705 polycondensation of fatty acid-based AB<sub>n</sub>-type monomers. *Green Chemistry* 19, 259-  
706 269. <https://doi.org/10.1039/C6GC02294D>
- 707 Tran, T.-N., Guyomard-Lack, A., Cerclier, C., Humbert, B., Colomines, G., Pilard, J.-F., Deterre, R.,  
708 Bideau, J.-L., Leroy, E., 2018. Natural rubber-based ionogels. *J. Renew. Mater.* 6, 251-  
709 258. <https://doi.org/doi:10.7569/JRM.2017.634174>
- 710 Valeska Zeisler-Diehl, V., Migdal, B., Schreiber, L., 2017. Quantitative characterization of cuticular barrier  
711 properties: methods, requirements, and problems. *J. Exp. Bot.* 68, 5281-  
712 5291. <https://doi.org/10.1093/jxb/erx282>
- 713 Wang, Y., Gupta, M., Schiraldi, D.A., 2012. Oxygen permeability in thermoplastic polyurethanes. *J.*  
714 *Polym. Sci. Pol. Phys.* 50, 681-693. <https://doi.org/10.1002/polb.23053>
- 715 Yeats, T.H., Rose, J.K., 2013. The formation and function of plant cuticles. *Plant Physiol.* 163, 5-  
716 20. <https://doi.org/10.1104/pp.113.222737>

718

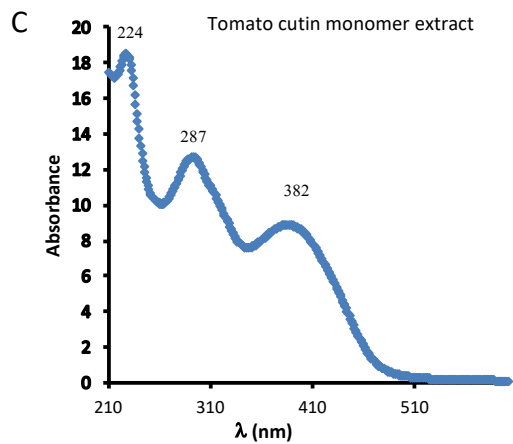
719

720

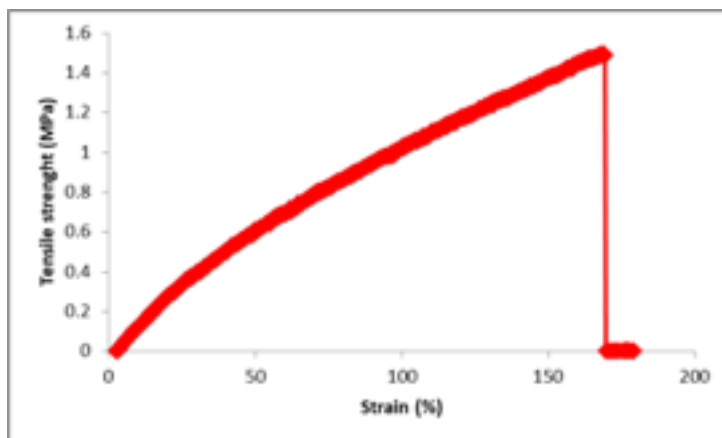


**B**

cutin monomers batch composition	%	(s.d.)
p-coumaric acid	1.8	(0.3)
16-hydroxy-hexadecanoic acid	2.7	(0.4)
16,9(10)-dihydroxyhexadecanoic acid	92.2	(2.3)
Hexadecane-1,16-dioic acid	0.4	(0.03)
7/8-hydroxy hexadecan-1,16-dioic acid	2.9	(1.2)



**Supplemental Figure 1** – Composition and characterization of the cutin monomer extracted from tomato cutin from industrial tomato peels  
 A. Cutin monomer composition. Value are means (standard deviation) of three experiments. B. FTIR spectrum. C. UV spectrum



**Supplemental Figure 2 – Elastomeric recovery cutin-inspired polyesters**

On the left, image of elastomeric sample (PG0.4) before and after mechanical test (right) showing its total shape recovery

722